Phosphate limitation triggers Fe^{3+}-dependent polymyxin resistance in *Enterobacteriaceae*

Guangming Zhang[1], Ziqing Deng[1,2,8], Jiezhang Jiang[3,4,8], Minji Wang[1,5], Xiaoyuan Wang[6,7]*, Xiaoyun Liu[3,4]*, Aixin Yan[1]*

[1] School of Biological Sciences, Faculty of Science, The University of Hong Kong, Hong Kong SAR, China

[2] Present address: BGI Research, Beijing, China.

[3] Department of Microbiology and Infectious Disease Center, NHC Key Laboratory of Medical Immunology, School of Basic Medical Sciences, Peking University Health Science Center, Beijing, China

[4] Department of Infectious Diseases, Peking University Third Hospital, Beijing, China

[5] Present address: School of Chemistry and Material Sciences, University of Shanghai for Science and Technology, Shanghai, China.

[6] State Key Laboratory of Food Science and Resources, Jiangnan University, Wuxi, China

[7] School of Biotechnology, Jiangnan University, Wuxi, China

[8] These authors contributed equally to this work: Ziqing Deng, Jiezhang Jiang

* Correspondence: Xiaoyuan Wang: xwang@jiangnan.edu.cn; Xiaoyun Liu: xiaoyun.liu@bjmu.edu.cn; Aixin Yan: ayan8@hku.hk.

Abstract

Phosphate (Pi) limitation is a pervasive stressor in bacterial habitats that often promotes increased antibiotic resistance. However, the ecophysiological drivers and regulatory mechanisms remain largely unresolved, impeding targeted interventions. Here, we identify a conserved Pi–Mg–Fe–PmrAB signalling pathway in *Enterobacteriaceae* that mediates Pi starvation-induced resistance to polymyxin B, a last-resort antibiotic. We demonstrate that Pi depletion disrupts Mg^{2+} homeostasis, leading to Fe^{3+} mobilization to cell membrane, which activates PmrAB and the downstream *arnABCDTEF* operon. This system catalyzes L-Ara4N modification of lipid A, a universal component of Gram-negative outer membranes, conferring polymyxin resistance. Unlike phosphorus-free lipid strategies in *P. aeruginosa*, the Mg–Fe–PmrAB pathway is druggable. We show that Mg^{2+} supplementation or Fe^{3+} chelation effectively reverses resistance. Phylogenetic analyses reveal species-specific differences in PmrB sensing capabilities, highlighting the importance of understanding regulatory diversity. Our findings uncover a conserved mechanism of stress-induced resistance, offering new avenues for resistance management.

Introduction

Nutrient scarcity is a pervasive challenge in microbial habitats, promoting the evolution of bacterial survival strategies and shaping community structures and functions (Fang *et al*, 2016; Poole, 2012). Among the macronutrients essential for bacteria, phosphorus (P) serves as a critical element for life. It is a fundamental component of key biomolecules such as nucleic acids, phospholipids, and ATP, and plays crucial roles in the essential processes of genetic inheritance, energy metabolism, membrane integrity, and signal transduction (Fagerbakke *et al*, 1996; Wanner, 1996). The primary assimilable form of phosphorus for bacteria is the orthophosphate anion (PO_4^{3-}), commonly known as

inorganic phosphate (Pi). However, Pi is typically found at very low concentrations (<4μM) in various ecosystems, such as oceans (0.1-3μM) (Moore *et al*, 2013; Van Mooy *et al*, 2009) and soil (0.0105 to 10.5μM, <1μM near plant roots) (George *et al*, 2016; Vitousek *et al*, 2010), and host-associated environments such as macrophages (<4μM) (Eriksson *et al*, 2003) and sputum of cystic fibrosis patients (<4μM) (Jones *et al*, 2021), etc. To cope with Pi scarcity and survive under these conditions, bacteria have evolved a conserved global regulatory system known as the phosphate (Pho) regulon, governed by the two-component system PhoBR. This system is activated when extracellular Pi concentrations fall below 4 μM, triggering the response regulator PhoB to bind PHO boxes and upregulate genes involved in Pi acquisition, transport, and storage (Amemura *et al*, 1985; Hsieh & Wanner, 2010; Makino *et al*, 1989; Shinagawa *et al*, 1983; Stock *et al*, 1989; Wanner, 1996).

In addition to Pi assimilation, Pi starvation is known to often trigger broader adaptive responses such as enhanced virulence and antibiotic resistance (Chekabab *et al*, 2014a; Crépin *et al*, 2011; Lamarche *et al*, 2008; Romano *et al*, 2015; Santos-Beneit, 2015). For instance, in pathogens such as *Vibrio cholerae*, enterohemorrhagic *Escherichia coli* (EHEC), and *Pseudomonas aeruginosa*, Pi limitation induces the upregulation of virulence factors such as the toxin-coregulated pilus (TCP) and cholera toxin (CT) in *V. cholerae* (Pratt *et al*, 2010), the locus of enterocyte effacement (LEE) in EHEC (Chekabab *et al*, 2014b), and pyocyanin production in *P. aeruginosa* (Jensen *et al*, 2006). Consequently, deletion of the Pi-specific transporter system (Δ*pst*) in *V. cholerae* and enteropathogenic *E. coli* (EPEC) resulted in impaired colonization in infant mice and reduced virulence, respectively (Cheng *et al*, 2009; Ferreira & Spira, 2008). Supplementing excess Pi protected mice from *P. aeruginosa* infection (Romanowski *et al*, 2011).

Beyond promoting virulence, Pi starvation has also been widely reported to induce antimicrobial resistance across diverse bacteria taxa, particularly against cationic

antibiotics. For instance, the soil-dwelling bacterium *Streptomyces coelicolor* exhibits increased resistance to vancomycin under Pi-limitation condition (Santos-Beneit & Martin, 2013). Several ubiquitous and clinically significant bacteria, including *Pseudomonas fluorescens, Pseudomonas aeruginosa* and *Acinetobacter baumannii*, also demonstrate enhanced resistance to the cationic antibiotic polymyxin B or polymyxin E, when subjected to Pi limitation (Dorrer & Teuber, 1977; Jones *et al.*, 2021; Lewenza *et al*, 2011; Olea-Ozuna *et al*, 2025). However, the regulatory mechanisms underlying the Pi starvation-induced antimicrobial resistance remain largely unexplored. Recent study began to shed light on these process: Jones et. al. reported that in *P. aeruginosa*, Pi limitation induced polymyxin B resistance through activating the synthesis of phosphorus-free, neutral lipids, such as monoglucosyl diacylglycerol (MGDG) and glucuronic acid diacylglycerol (GADG), which replace the negatively charged phospholipids in the membrane (Jones *et al.*, 2021). Similarly, Olea-Ozuna et. al. found that in *A. baumannii*, Pi limitation promoted polymyxin E resistance via the activation of phosphorus-free, positively charged ornithine- and lysine-containing aminolipids (OL and LL) biosynthesis (Olea-Ozuna *et al.*, 2025). However, these mechanisms are not universal, as MGDG/GADG pathways are predominantly found in Gram-positive bacteria and cyanobacteria (Feige *et al*, 1980; Kiriukhin *et al*, 2001), while OL biosynthesis genes are present in only approximately 25% bacterial genomes (Sohlenkamp & Geiger, 2016; Vences-Guzman *et al*, 2012). This raises the question of whether additional, yet unidentified mechanisms underlie Pi starvation-induced polymyxin resistance in other ecologically and clinically important bacteria, such as the clinically significant *Enterobacteriaceae* family, which largely lacks the OL and MGDG/GADG pathways.

In this study, we report that Pi limitation also induces polymyxin resistance in *Enterobacteriaceae*. Using *E. coli* K-12 MG1655 as a model, we demonstrate that Pi starvation induces polymyxin resistance through a distinct mechanism involving the modification of lipid A, a universal component of the outer membrane of all Gram-negative bacteria. This process results from the upregulation of the conserved Ugd

and ArnBCADTEF proteins which catalyze the addition of the positively charged 4-amino-4-deoxy-L-arabinose (L-Ara4N) to lipid A. We show that this adaptive lipid A modification is driven by the loss of membrane-stabilizing magnesium (Mg^{2+}) and a compensatory iron (Fe^{3+}) mobilization to the cell membrane, leading to the activation of the PmrAB two-component regulatory system and its downstream gene *ugd-arn*. Importantly, interfering with the Pi-Mg-Fe-PmrAB circuit, ether by Mg^{2+} supplementation or iron chelation, effectively offset the resistance in representative *Enterobacteriaceae* species. Conversely, such interventions fail to reverse resistance in non-enteric species like *P. aeruginosa*. Phylogenetic analyses reveal that PmrB from *E. coli* (EcoPmrB) and *P. aeruginosa* (PaePmrB) are clustered in distinct clades, with PaePmrB lacking the conserved "ExxE" motif required for Fe^{3+} sensing. Our findings uncover a conserved regulatory mechanism underlying Pi starvation-induced polymyxin resistance within *Enterobacteriaceae* and identify a stress responsive circuit that can be targeted for managing stress-induced resistance.

Results

Pi limitation induces polymyxin resistance in *Enterobacteriaceae*

To investigate whether Pi limitation induces antibiotic resistance in *Enterobacteriaceae*, we assessed the survival of representative species, *E. coli* MG1655 and *Salmonella enterica* serovar Typhimurium ATCC14028, against antibiotics following acute starvation in Pi-depleted MOPS medium (Pi-, 0 mM) for three hours, compared to control groups that were not subjected to Pi starvation (Pi+, 1.32 mM) (Fig. EV1). We observed that Pi depletion enhanced the survival of both species against the cationic antibiotic polymyxin B (Fig. 1A). Similar Pi starvation-induced polymyxin resistance was also observed in *E. coli* O157 and four uropathogenic *E. coli* strains isolated from urinary tract infection patients in the Queen Mary Hospital, Hong Kong (Fig. 1B). Consistent with previous reports, *P. aeruginosa* PAO1 subjected to Pi starvation also display enhanced resistance

to polymyxin B (Fig. 1B). These results suggest that Pi starvation-induced polymyxin resistance is a widespread phenomenon among Gram-negative bacteria.

Pi limitation induces 4-amino-4-deoxy-L-arabinose (L-Ara-4N) modification of lipid A in *Enterobacteriaceae*

Since these species lack the MGDG/GADG and OL pathways described in *P. aeruginosa* and *A. baumannii*, we employed *E. coli* K-12 MG1655 as a model to comprehensively investigate the regulatory mechanisms underlying this stress-induced polymyxin resistance. We performed quantitative proteomic analysis on *E. coli* cells subjected to phosphate-depletion (Pi- MOPS medium) for 3 hrs, compared to cells grown under Pi sufficient conditions in standard MOPS synthetic medium (Pi concentration 1.32 mM) (Fig. EV1). Among the 2990 proteins detected which cover 69% of the 4358 proteins annotated in the UniProt *E. coli* MG1655 database, abundance of 225 proteins was found to be altered during Pi starvation, with 142 proteins upregulated and 83 downregulated (Fig. EV2) (Appendix Table. S1). In addition to proteins belonging to the Pho regulon, such as PhoB, PstB, PhoU, and PhnB (Fig. 2A) in the COG functional group of transportation and metabolism of inorganic ions (13% of upregulated proteins) (Fig. EV2), the most abundant functional groups among the significantly upregulated proteins include those involved in cell wall/membrane/envelope biogenesis (13%) and energy production and conversion (10%) (Fig. EV2). Conversely, proteins involved in translation, ribosomal structure and biogenesis (33%) and amino acid transport and metabolism (17%) were significantly downregulated (Fig. EV2).

Specifically, among the most upregulated proteins ($\log_2$FC>10) induced by Pi limitation (Appendix Table. S1), two proteins encoded in the *arnBCADTEF* operon: ArnB and ArnC, were identified (Figs. 2A and 2B). Additionally, two other proteins in the Arn pathway, ArnA and Ugd, were also up-regulated with more than five-fold in response to Pi starvation (Figs. 2A and 2B). This finding is particularly intriguing, because Ugd and Arn proteins are known to catalyze the biosynthesis of 4-amino-4-deoxy-L-arabinose

(L-Ara4N) and its modification of lipid A (Fig. 2B), which confers resistance to the cationic antibiotic polymyxins due to simultaneous neutralization of a negative charge and introduction of a positive charge to lipid A (Raetz *et al*, 2007). To verify the upregulation of these proteins, we first examined the mRNA level of *ugd* and *arnB* genes by RT-qPCR and found their levels were 16- and 27-fold higher, respectively, under Pi- than under Pi+ conditions (Fig. 2C). Next, we constructed ArnB-3×FLAG in MG1655 chromosome and observed a significant production of the ArnB protein under Pi- conditions, while its level was undetectable under Pi+ conditions (Fig. 2D). We also constructed promoter-*lacZ* fusions and observed more than 10-fold higher promoter activities for both *ugd* and *arn* genes under Pi- conditions than Pi+ conditions (Fig. 2E), confirming the upregulation of the Ugd-Arn system under Pi depletion.

We then extracted lipid A molecules from *E. coli* MG1655 cells cultured under identical conditions as in the polymyxin challenging assay and the proteomic analysis, and analyzed the extract using ESI-MS. Native lipid A, a hexacetylated glucosamine disaccharide with two phosphate groups at position 1 and 4’ (m/z 1796.98), was detected in *E. coli* cells cultured under Pi sufficient conditions (Fig. 2F). In constant, the predominant lipid A species in *E. coli* cells subjected to Pi depletion were found to be modified with L-Ara4N (m/z 1928.67) (Fig. 2F). Next, we deleted *arnT*, *arnB*, and *ugd* and found that deletion of these genes abolished Pi starvation-induced polymyxin B resistance in *E. coli* (Fig. 2G).

The induction of L-Ara4N modified lipid A, along with decrease in the unmodified form, was also observed in *E. coli* O157 (Fig. EV3A), a representative UTI strain UTI-3 (Fig. EV3B), and *S.* Typhimurium ATCC14028 (Fig. EV3C), each exhibiting varying ratios. These fundings indicate that L-Ara4N modification of lipid A is widespread in *Enterobacteriaceae* and correlates with increased resistance to polymyxin B. We also analyzed lipid A species in *P. aeruginosa* PAO1 and found that instead of the L-Ara4N modification, a 2-hydroxymyristate modification of lipid A, which is catalyzed by the

aspartyl beta-hydroxylase LpxO, was detected in Pi-depletion treated cells (Fig. EV3D). Altogether, these results indicated that unlike the strategy observed in PAO1 where Pi starvation induces resistance by replacing the negatively charged phospholipids with MGDG/GADG, in *E. coli*, resistance is mediated by lipid A modification with L-Ara4N catalyzed by Ugd and Arn proteins.

The PmrAB two component system is activated to up-regulate the *arn* operon during Pi starvation

To investigate how the *ugd-arn* genes were up-regulated during stress response to Pi limitation, we first deleted the global regulator genes *phoB* and *phoR* and measured the promoter activities of P_{ugd}-*lacZ* and P_{arn}-*lacZ.* Surprisingly, transcription from the *ugd* promoter decreased by only 30% (Fig. EV4), and there was no change in the *arn* promoter activity (Fig. 3A). This suggests that other regulatory systems are responsible for the upregulation of *arn* genes under Pi starvation conditions. It has been reported that transcription of the *arn* operon and *ugd* in *E. coli* is subjected to regulation by the PmrAB two-component system (TCS) (Ogasawara *et al*, 2012) under stress conditions of high Fe^{3+} level (Winfield & Groisman, 2004). To determine whether the upregulation of these genes observed under Pi starvation conditions is also dependent on PmrAB, we construct Δ*pmrB* and Δ*pmrA* and found that the upregulation of the *arn* operon under Pi starvation was abolished in these mutants (Fig. 3A). This suggests that the Arn system was activated by the PmrAB regulatory system in response to an as-yet-unidentified secondary signal induced by Pi starvation, rather than by Pi depletion itself. In line with this, deletion of *pmrB* or *pmrA* abolished the enhanced polymyxin B resistance observed in Pi-starved *E. coli* cells, whereas deletion of *phoB* or *phoR* had no effect (Fig. 3B). Regarding *ugd*, its promoter activity was unaffected in Δ*pmrB* and Δ*pmrA* mutants (Fig. EV4), suggesting that *ugd* is primarily regulated by PhoBR system during Pi starvation.

To assess whether PmrAB activation occurs under Pi depletion, we examined the phosphorylation of the response regulator PmrA using Phos-tag SDS-PAGE. As a

positive control, cells treated with excessive Fe^{3+} (>100μM) under Pi sufficient conditions (Wösten *et al*, 2000) showed increased PmrA phosphorylation in a Fe^{3+} dose-dependent manner (Fig. 3C, left panel). Notably, phosphorylated PmrA was also detected in cells subjected to Pi starvation without Fe^{3+} excess (Fig. 3C, right panel), demonstrating that Pi limitation activates PmrAB TCS. To confirm this in vivo, we performed a FRET-based whole-cell transcription factor-promoter binding assay (Wang *et al*, 2022). We incorporated a bright fluorescent unnatural amino acid, L-(7-hydroxycoumarin-4-yl) ethylglycine (CouA) (Wang *et al*, 2006) at position G137 within the DNA-binding domain of PmrA through genetic encoding, allowing it to serve as the FRET donor (Fig. 3D) (Wang *et al.*, 2022). The nucleic acid dye SYTO9 was utilized to stain promoter DNA of PmrA regulon (Fig. 3D) (Wang *et al.*, 2022), acting as the FRET acceptor. The whole-cell FRET assay revealed that, similar to the treatment with excessive $FeSO_4$ (500μM), a FRET signal indicative of PmrA binding to its target promoters was observed in cells subjected to Pi starvation without excessive $FeSO_4$ (Fig. 3E). These results confirmed that Pi starvation induced activation of the PmrAB signal transduction system in *E. coli.*

Elevated Fe^{3+} levels activate PmrAB and induce expression of downstream *arn* genes during Pi starvation response

PmrAB has been previously reported to be activated by ferric ion (Fe^{3+}), aluminum ion (Al^{3+}), or acidic pH (Chen & Groisman, 2013). Since no Al^{3+} was added in the culture, and the pH remained largely unchanged (7.2-7.0) across the Pi depletion treatments (Fig. EV5), we focused on Fe^{3+} as the likely activation signal. The mechanism by which EcoPmrB senses the inducing signal remains unclear. However, in *S.* Typhimurium, the homologue of PmrB (StPmrB) senses Fe^{3+} through four conserved glutamic acid residues ($E^{36}xxE^{39}$ and $E^{61}xxE^{64}$) in its periplasmic domain (Perez & Groisman, 2007; Wösten *et al.*, 2000). To test whether *E. coli* PmrB functions similarly during Pi starvation, we constructed chromosomal *pmrB*^{E36A} and *pmrB*^{E39A} mutations in *E. coli* MG1655 (Fig. 4A). β-galactosidase activity assay revealed that these mutations abolished the

response of P_{arn}-*lacZ* reporter to Fe^{3+} excess (100μM) (Fig. EV6), confirming that the two conserved amino acids are essential for Fe^{3+} sensing by EcoPmrB. Notably, both mutations also abolished the upregulation of *arn* transcription under Pi starvation (Fig. 4B), indicating that activation of the PmrAB TCS under this condition is dependent on its capability of sensing Fe^{3+}, a potential secondary stress signal induced by Pi depletion.

Next, we measured cellular iron (Fe) levels using ICP-MS. Cells subjected to Pi starvation for 3 hrs exhibited a more than 5-fold increase in Fe content compared to initial levels at the onset of starvation (Fig. 4C). In constrast, cellular copper (Cu), zinc (Zn), and calcium (Ca) levels remained unchanged (Fig. 4C). correspondingly, Fe content in the spent medium of Pi starved cells decreased relative to that at the onset of Pi starvation (Fig. 4D), indicating Fe mobilization from the medium to *E. coli* cells during the stress adaptation process.

To confirm the role of Fe mobilization in activating PmrAB during Pi starvation, we treated cells with Fe-free, Pi depleted MOPS medium and found that the upregulation of the *arn* operon was abolished (Fig. 4E). Upon varying amounts of Fe were reintroduced P_{arn}-*lacZ* activity increased in a Fe dose-dependent manner (Fig. 4F), further confirming Fe mobilization from medium to *E. coli* cells during Pi starvation and its role to activate PmrAB and *arn* genes. Notably, *arn* activation occurred at much lower medium Fe concentration (~10-fold less) in Pi-starved cells compared to Pi-sufficient conditions (Fig. 4F), suggesting enhanced Fe mobilization under Pi limitation.

Elevated cellular Fe during Pi starvation is mediated by Fe association to cell membrane

To explore how Fe is mobilized during Pi starvation, we first deleted genes involved in canonical iron uptake in *E. coli*, i.e., *fecA*, *fepA*, *fiu*, *cirA*, and *entE*, which encoded outer membrane endogenous iron-chelator complex receptors and enterobactin synthetase. Surprisingly, P_{arn}-*lacZ* activity remained induced in these mutants and in the

262 penta-deletion mutant (Δ5Fe) lacking all five genes (Fig. EV7A). ICP-MS analysis
263 confirmed that cell-associated Fe still increased by more than 5-fold in Δ5Fe under Pi
264 starvation (Fig. EV7B). These results suggested that Fe-mediated activation of PmrAB
265 under Pi starvation was not due to enhanced intracellular Fe uptake.

266 Since PmrAB primarily senses periplasmic and cell surface-bound Fe^{3+} (Wösten *et al.*,
267 2000), we investigated Fe association with cell surfaces during Pi starvation. The outer
268 leaflet of the Gram-negative bacteria outer membrane (OM) primarily comprises lipid A,
269 which bears two negatively charged phosphate groups at 1 and 4′ positions. These
270 negative charges are typically neutralized by cell-associated Mg^{2+} and Ca^{2+} to maintain
271 membrane stability (Alves *et al*, 2016). Interestingly, we observed a 44% decrease of Mg
272 content in *E. coli* cells after 3 hrs of Pi starvation, while Ca^{2+} levels remained unchanged
273 (Fig. 4C). Monitoring the dynamic Mg and Fe levels over time revealed that Mg
274 decreased progressively upon transferring *E. coli* cells to Pi-depleted medium which
275 continued during the test window of five hours (Fig. 5A). The loss of Mg^{2+} was found to
276 be independent of Fe, as the same degree of loss occurred in *E. coli* cells exposed to
277 Fe-free Pi-depleted medium (Fig. EV8). Conversely, cellular Fe increased, peaking after
278 two hours of Pi starvation before slightly declining (Fig. 5A). The dynamics of Fe
279 accumulation correlated with P_{arn}-*lacZ* activities (Fig. 5B), suggesting Fe is actively
280 mobilized to the cell surface during Pi starvation, likely to compensate for Mg^{2+} loss and
281 stabilize the membrane during Pi starvation. The subsequent activation of the PmrAB
282 and Arn system may represent an adaptation response to physiological changes during
283 Pi starvation, likely disruption of OM stability caused by Mg^{2+} dissociation. Supporting
284 this notion, deletion of *pmrA* led to an even greater and sustained increase in Fe
285 mobilization during Pi starvation (Fig. 5C), which could be toxic to *E. coli* cells.

286 To directly assess Fe association to the cell surface during Pi starvation, we
287 supplemented the cell-pellet washing buffer with deferoxamine (DFOM), a
288 membrane-impermeable Fe^{3+} specific chelator (Breuer *et al*, 1995). ICP-MS analysis

showed that DFOM reduced Fe content significantly in cells from Pi-starved cultures, but had little effect on cells from Pi-replete cultures (Fig. 5D). Quantification revealed that Pi starved cells experienced a 2-fold greater Fe loss upon DFOM washing compared to than cells collected fro Pi sufficient cells (Fig. 5E). These results demonstrated that Pi starvation promoted Fe mobilization to cell surfaces, which was susceptible to removal by membrane impermeable Fe^{3+} chelator.

Enhanced Fe^{3+} mobilization to cell surfaces is driven by Mg^{2+} loss during Pi starvation

To understand the driving force behind enhanced Fe mobilization during Pi starvation, we supplemented the culture medium with excess Mg (10mM) to counteract Mg loss during the process. As expected, this supplementation significantly reduced Fe mobilization to MG1655 cells during Pi starvation (Fig. 6A), and correspondingly P_{arn}-*lacZ* activity declined as the Mg concentration increased in the Pi-depleted medium (Fig. 6B). These results strongly suggest that Fe mobilization to the cell surface during Pi starvation depends on Mg^{2+} loss. We further monitored Mg^{2+} dynamics in the spent medium of *E. coli* cells subjected to Pi starvation and observed a continuous increase in Mg levels following transfer to Pi-depleted condition (Fig. 6C). Similar Mg^{2+} release was also observed in the spent medium of cells cultured in Mg^{2+}-free, Pi-depleted medium (Fig. EV9). These results suggested that although Mg^{2+} is essential for bacterial growth, under Pi starvation, its imbalance with phosphorus may lead to active Mg^{2+} dissociation from the cells. A comparable degree of Mg^{2+} loss (45%) was also observed in *P. aeruginosa* PAO1 cells under similar conditions (Fig. EV10). However, the extent of Fe mobilization following Pi-depletion was less pronounced (2.4-fold compared to 5.4-fold in *E. coli*) (Fig. EV10), reflecting a different adaption strategies in this species, predominantly activation of the MGDG/GADG pathways (Jones *et al.*, 2021).

Given that membrane-associated Mg^{2+} primarily neutralizes the negative charges of lipid A to stabilize the OM, we hypothesize that Mg^{2+} loss during Pi starvation alters OM

properties, while Fe mobilization to the cell may serve to stabilize the OM under this condition. To test this, we applied an OM-sensitive probe (Long *et al*, 2019) to assess the physiochemical features of *E. coli* OM during Pi starvation. The 2D sensor output revealed distinct signals between cells grown with sufficient Pi and those under Pi limitation (Fig. 6D), indicating a change in OM characteristics. Notably, cells in Fe-free, Pi-depleted medium exhibited even greater shifts (Fig. 6D), suggesting that Fe mobilization and subsequent activation of the PmrAB-Arn pathway served as an adaptation strategy to maintain OM integrity during Pi stress. This strategy likely prevents uncontrolled Fe accumulation and toxicity during Pi starvation (Wösten *et al.*, 2000), ultimately resulting in stress-induced polymyxin resistance. A schematic model illustrating this stress adaptation process and its impact on polymyxin resistance is presented (Fig. 7).

Disrupting the Mg-Fe-PmrAB-Arn circuit counters Pi starvation-induced polymyxin resistance in *Enterobacteriaceae*

Our findings above identified a Mg-Fe-PmrAB-Arn circuit underpinning the polymyxin resistance induced by stress adaptation to Pi starvation. To evaluate whether interference with this pathway could mitigate the stress-induced polymyxin resistance, we supplemented Pi-starved culture with excess Mg^{2+} (10mM) or applied a membrane impermeable chelator DFOM (10μM). Both approaches effectively suppressed Pi starvation-induced polymyxin resistance in *E. coli* and *S.* Typhimurium (Fig. 8A). In contrast, neither intervention reversed polymyxin resistance in *P. aeruginosa* despite various combinations of Mg^{2+} supplementation and Fe chelation (Fig. EV11). This highlights species-specific adaptative strategies and aligns with several observations from our study as well as several previous research (Huang *et al*, 2020; Jones *et al.*, 2021). Specifically, in *P. aeruginosa,* despite a 45% Mg loss during Pi starvation, Fe levels increased only two-fold compared to over five-fold in *E. coli*, consistent with its reliance on MGDG/GADG lipids synthesis regulated by the PhoBR system (Fig. 8B)

(Jones *et al.*, 2021). Additionally, *P. aeruginosa* exhibits a distinct lipid A modification, 2-hydroxy myristate (Fig. EV3D), that does not confer polymyxin resistance (Hofstaedter *et al*, 2024). Phylogenetic analysis of 250 PmrB homologs revealed that EcoPmrB and PaePmrB cluster in separate clades, with PaePmrB lacking the conserved "ExxE" motif essential for Fe^{3+} sensing (Fig. 8C). Together, these findings underscore the diverse stress response strategies employed by different classes of Gram-negative bacteria and highlight the importance of understanding species-specific regulatory mechanisms for developing targeted interventions against stress-induced antibiotic resistance.

Discussion

It has long been reported that Pi starvation induces resistance to cationic antimicrobial agents across diverse bacterial species (Dorrer & Teuber, 1977; Jones *et al.*, 2021; Lewenza *et al.*, 2011). However, the ecophysiological drivers and the molecular mechanisms underlying this phenomenon have remained largely unresolved, particularly with respect to species-specific adaptation pathways. In this study, we identify a conserved mechanism in *Enterobacteriaceae*, whereby L-Ara4N modification of lipid A, a ubiquitous component of the Gram-negative outer membrane, governs Pi starvation-induced resistance to polymyxin B. Notably, we discovered that Pi limitation triggers a secondary signal: increased Fe^{3+} mobilization to the cell surface, a process driven by Mg^{2+} dissociation under Pi-depleted conditions. This Fe^{3+} signal activates the PmrAB two-component system, leading to the upregulation of the *arn* operon and subsequent L-Ara4N modification of lipid A (Fig. 7). Thus, *Enterobacteriaceae* utilize a distinct regulatory pathway whereby Pi starvation is transduced via cationic imbalance and Fe^{3+} signaling to remodel the outer membrane, revealing an ecophysiological vulnerability that can be exploited to mitigate resistance mitigation.

In bacteria, ATP and rRNA serve as the primary cytoplasmic reservoirs for both Pi and Mg^{2+} (Bruna *et al*, 2021; Gesteland, 1966; Gillooly *et al*, 2005; Klein *et al*, 2004; Pontes & Groisman, 2018; Pontes *et al*, 2015), with maintaining a balanced P/Mg ratio being essential for optimal growth and function. Previous research by Bruna et al. showed that bacteria suppress Pi uptake under Mg^{2+} limitation to preserve cellular physiology (Bruna *et al.*, 2021). Here, we extend this concept by showing that Pi scarcity itself triggers Mg^{2+} release, thereby highlighting the tightly coupled regulation of Pi and Mg^{2+} homeostasis. Our proteomic analysis further revealed that proteins involved in translation, ribosomal structure, and biogenesis were among the most significantly downregulated groups during Pi starvation (Figs. 1A and EV3). Consistently, we found that cellular ATP levels declined steadily under Pi-limited conditions (Fig. EV12), suggesting an arrest in ribosome biogenesis and protein synthesis that may contribute to Mg^{2+} release and loss from the cell.

In *Enterobacteriaceae*, Mg^{2+} homeostasis is primarily governed by the PhoPQ two-component system (Perez *et al*, 2009), which is well-characterized in *Salmonella* Typhimurium, where PhoPQ is activated under low extracellular Mg^{2+} conditions (Groisman *et al*, 1989; Véscovi *et al*, 1996). To assess whether Mg^{2+} dissociation during Pi starvation activates PhoPQ in *E. coli*, we monitored the transcription of its regulon genes *phoQ* and *mgtA* using promoter-*lacZ* reporters. Neither gene was upregulated during Pi starvation (Fig. EV13), indicating that although Mg^{2+} is lost from the cell, the loss is insufficient to trigger the canonical PhoPQ response. Instead, our data suggest that under acute Pi starvation, *Enterobacteriaceae* preferentially engage an Fe^{3+}-mediated membrane remodeling pathway, which activates the *arn* operon and L-Ara4N modification independently of the classical Mg^{2+}-sensing pathway.

Notably, this Fe^{3+}-mediated lipid A modification strategy is distinct from that employed by *P. aeruginosa*, where Pi starvation-induced polymyxin resistance is governed by the PhoBR regulon. PhoBR directly senses Pi depletion and activates the expression of

genes responsible for the biosynthesis of phosphorus-free glycolipids, specifically MGDG and GADG, which replace the negatively charged phospholipids under Pi-limiting conditions (Fig. 8B) (Jones *et al.*, 2021). Although *P. aeruginosa* also possesses a PmrAB homologue, its PmrB sensor kinase lacks the Fe^{3+}-sensing "ExxE" motifs present in *Enterobacteriaceae* PmrB and cannot directly respond to Fe^{3+}. Instead, PmrAB activation in *P. aeruginosa* depends on the PhoPQ system, which senses low extracellular Mg^{2+}. Consequently, in *P. aeruginosa*, primary Pi starvation response involves PhoBR-regulated MGDG/GADG biosynthesis to mitigate membrane perturbations, whereas *Enterobacteriaceae* lacking MGDG/GADG pathways rely on a secondary Fe^{3+}-sensing mechanism. Here, the PmrAB system, with its Fe^{3+}-sensing "ExxE" motifs in PmrB, orchestrates membrane remodeling via upregulating L-Ara4N modification of lipid A as a physiological adaptation to Pi starvation (Huang *et al.*, 2020). Moreover, while lipid A modification was detected in *P. aeruginosa* during Pi starvation, they involve the addition of 2-hydroxymyristate (catalyzed by LpxO), which does not contribute to polymyxin resistance (Hofstaedter *et al.*, 2024). Notably, *lpxO* expression is not regulated by PhoBR, PhoPQ, or PmrAB. Hence, this modification appears to serve other physiological functions, independent of antibiotic resistance.

The biosynthesis of L-Ara4N and its transfer to lipid A are mediated by Ugd and ArnABCDEFT proteins, encoded by the *ugd* gene and the *arn* operon, respectively (Breazeale *et al*, 2005; Breazeale *et al*, 2002, 2003; Trent *et al*, 2001; Yan *et al*, 2007). Our data reveal that, during Pi starvation, the *arn* transcription is tightly controlled by the PmrAB system, whereas *ugd* expression is not dependent on PmrAB and is partially controlled by the PhoBR system (Fig. EV4). This regulatory separation is not unexpected: *ugd* encoded UDP-glucose dehydrogenase, which plays dual roles in L-Ara4N biosynthesis (Gunn *et al*, 1998) and in exopolysaccharide production such as colanic acid (Stevenson *et al*, 1996). Consequently, while PmrAB activation of *arn* is critical for L-Ara4N modification of lipid A during Pi limitation, *ugd* regulation reflects its broader involvement in cellular metabolism and stress responses.

In both natural habitats and in host-related niches, Pi scarcity imposes dual challenges: nutrient acquisition and defense against antimicrobial threats. In line with the widespread presence of *Enterobacteriaceae* across diverse hosts and environments (Dahal, 2022), the Pi-Mg-Fe-PmrB regulatory circuit we uncovered may facilitate the adaptation of these bacteria to highly heterogeneous environments with fluctuating Pi levels during host colonization, transmission, or environmental survival. In addition, Pi-Mg-Fe-PmrAB-mediated membrane remodeling may enable bacteria to preserve membrane integrity and withstand cationic antimicrobial peptides (CAMPs) produced by competing microbes or host defenses.

Taking together, our findings elucidate a conserved regulatory circuit in *Enterobacteriaceae* that is distinct from those characterized in *P. aeruginosa*. This circuit links Pi and Mg^{2+} homeostasis to Fe^{3+}-mediated lipid A modification, leading to stress-induced antibiotic resistance. Importantly, targeting this circuit effectively mitigated stress-induced resistance. Given that polymyxins remain the last-line antibiotics for treating Gram-negative bacterial infections, our study not only offers critical insights into the molecular mechanisms underlying stress-induced resistance but also highlights its potential for informing resistance management strategies.

Methods

Bacterial strains and growth conditions

Strains, plasmids, and primers used in this study are listed in the Appendix Tables S2 and S3. Bacteria were cultured in lysogeny broth (LB) broth/plates or MOPS minimal medium. MOPS medium was freshly prepared from 1× MOPS stock by supplementing 0.1 % (w/v) glucose and 1.32 mM K_2HPO_4. Acute Pi starvation was applied by transferring bacteria culture into the non-Pi MOPS medium. 1× MOPS consists of 40 mM MOPS, 4 mM Tricine, 10 μM $FeSO_4 \cdot 7H_2O$, 9.5 mM NH_4Cl, 0.276 mM K_2SO_4, 0.5 μM $CaCl_2 \cdot 2H_2O$, 525 μM $MgCl_2$, 50 mM NaCl, 0.003 μM $(NH_4)_6Mo_7O_{24}$, 0.4 μM H_3BO_3, 0.03 μM $CoCl_2$, 0.01 μM $CuSO_4$, 0.08 μM $MnCl_2$, and 0.01 μM $ZnSO_4$. Antibiotics applied to select and maintain the construct were chloramphenicol (25 μg/ml), kanamycin (20 μg/ml) and ampicillin (100 μg/ml).

Lipid A extraction and ESI-MS analysis

Lipid A was extracted from designated *E. coli* cells using Bligh-Dyer method as described (Bligh & Dyer, 1959; Reynolds & Raetz, 2009) with minor modifications. *E. coli* MG1655 cultured in MOPS medium to OD_{600} of 0.5 was harvested as cells under Pi sufficient condition. The same volume of cells was washed with Pi starvation medium for 3 times and resuspended in Pi starvation medium and shake for 3 hrs at 37°C as cells subjected to Pi starvation. 200 ml of each type of cell pellets with three biological replicates were harvested by centrifugation at 4500 rpm for 30 min and washed with H_2O. The cell pellets were suspended in 76 ml of a single-phase Bligh-Dyer mixture (chloroform: methanol: water=1:2:0.8; v/v/v) and stirred at room temperature for 1 h. Insoluble debris was collected by centrifugation at 4500 rpm for 30 min, washed with 60 ml single-phase Bligh-Dyer mixture, and suspended in 27 ml of 12.5 mM sodium acetate (pH 4.5). The mixture was heated at 100°C for 30 min and cooled to room temperature. The suspension was mixed with 30 ml chloroform and 30 ml methanol. Following vigorously

shaken for extraction of lipid A and centrifugation for 30 min, the lower phase containing lipid A was collected and dried with a rotary evaporator.

All the mass spectra of lipid A samples were acquired using Waters SYNAPT quadrupole time-of-flight mass spectrometer (MS) equipped with an electrospray ionization source (Sahonero-Canavesi *et al*). Lipid A samples were dissolved in a mixture of chloroform and methanol (4 : 1; v/v) and subjected to ESI/MS in the negative ion mode. Data acquisition and analysis were performed using MASS LYNX V4.1 software, Waters, Milford, MA, USA.

ICP-MS and DFOM treatment

Total cellular metal content was quantified using inductively coupled plasma mass spectrometry (ICP-MS) following previous description with minor modifications (Xu *et al*, 2019). *E. coli* cells equivalent to OD_{600} as 5 were harvested by centrifugation at 4500 rpm for 15 mins and washed three times with ice-cold PBS buffer. Cell pellets were subjected to acid digestion with 100 µl 65.0 % HNO_3 (Fluka) at 65°C for 16hrs. Samples were diluted to a final volume of 15 ml with 1% HNO_3 and subjected to ICP-MS detection on Agilent 7900 system (Agilent Technologies, CA). Samples were further diluted if the signals exceeded the liner range of standard curve. The standard curves of tested metals were generated from multi-element calibration standard-2A for ICP-MS (Agilent). Metal contents in bacteria were calculated based on the standard curve and results were normalized to original cell number.

Deferoxamine mesylate salt (sigma) were applied to examine the degree of iron association to *E. coli* cell surface. *E. coli* cells equivalent to OD_{600} as 5 were harvested by centrifugation at 4500 rpm for 15 mins. Cell pellets were resuspended in HEPES buffered saline with and without 50µM DFOM and incubated in 37°C for 30 mins with 220rpm agitation. Total cellular metal content of these treated cells was quantified using inductively coupled plasma mass spectrometry (ICP-MS) as described above.

OM feature monitoring using PI-BactD

OM feature of *E. coli* was monitored by an OM-sensitive probe PI-BactD following previous description with minor modifications (Long *et al.*, 2019). *E. coli* cells grown under designated conditions were harvested by centrifugation at 13000 rpm for 2 mins and washed with PBS buffer (10 mM, pH 7.2) twice. Cell pellets were resuspended in PBS buffer to an OD_{600} of 0.5. Fluorescence probe PI-BactD (gift from prof. Xu Z, Dalian) was added into 1mL cell suspension to a final concentration of 2 mM and incubated at room temperature for 1 min. Output signals of two channels: fluorescence increase ($\Delta S/S_0$) and fluorescence ratio metric changes (I_{482}/I_{375}) were recorded to plot the 2D graph (Thermo Scientific Varioskan® Flash spectral scanning multimode reader). Six replicates were conducted for each strain and treatment.

Construction of $P_{promoter}$-*lacZ* (P_{arn}-*lacZ* as example) fusion in the single-copy plasmid pNN387

A DNA fragment corresponding to the -200 to -1 region relative to the ATG start codon of *arnB* was amplified using *E. coli* MG1655 genomic DNA as the template and primers specific to this fragment flanked with NotI and HindIII restriction sites at the 5'- and 3'-end, respectively. Following digestion with NotI and HindIII and purification using the MiniBEST agarose gel DNA extraction kit (TaKaRa), the fragment was ligated into the plasmid pNN387 which was treated with the same restriction enzymes using the quick ligation kit (NEB). The resulting construct was selected on LB agar plates supplemented with chloramphenicol (25 μg/ml) and was verified by DNA sequencing (BGI, Shenzhen).

Beta-galactosidase activity assay

β-gal activity assay was performed based on a previous description (Xu *et al.*, 2019) with modifications. Cells were grown under designated conditions until OD_{600} reached 0.4. 10 μg/ml tetracycline was added to stop cell growth and protein synthesis, and cells were left

517 on ice until being assayed. 100μl of cell culture and 400 μl of Z buffer (60 mM Na_2HPO_4,
518 40 mM NaH_2PO_4, 10 mM KCl, 1 mM $MgCl_2$, 50 mM β-mercaptoethanol, pH 7.0, 4 °C)
519 were mixed. One drop of 0.1% SDS and two drops of chloroform were added to lyse the
520 cells. The reactions were initiated by adding 100 μl of 4 mg/ml
521 ortho-nitrophenyl-β-galactoside into cell suspension and were incubated at 28 °C. Color
522 development in the mixtures was monitored. Finally, 250μl of 1M Na_2CO_3 was added to
523 stop the reaction. Color of the mixtures were measured using spectrophotometer at
524 OD_{420} and OD_{550}. The expression value in Miller units was calculated, and results are
525 presented as the mean of three biological replicates.

526 **RNA extraction and RT-qPCR**

527 Bacterial cells grown under designated conditions was subjected to RNA extraction when
528 the OD_{600} reached 0.4. Cells were harvested by centrifugation at 4,500 rpm for 10 min at
529 4 °C. After removing the supernatant, the cell pellet was stored at -80 °C to aid cell lysis.
530 Total RNA was extracted using the MiniBEST Universal RNA Extraction Kit (Takara,
531 Japan) according to the manufacturer's instruction. Reverse transcription (RT) was
532 performed using PrimeScript^{TM} RT reagent Kit (Takara, Japan). Quantitative PCR was
533 performed using specific primers and the TB Green® Premix Ex Taq™ (Takara, Japan)
534 in a 20 μL reaction system. The reaction was performed in the ABI StepOnePlus real time
535 PCR system with *rrsB* as reference gene to normalize the relative expression of the
536 target genes. The results were presented as fold change expression of the target genes,
537 and results were presented as the mean of three biological isolates.

538 **Construction of clean gene deletion, point mutation and tag insertion in**
539 **chromosome of *E. coli* MG1655**

540 Gene deletion, mutation, and tag insertion in chromosomal were achieved employing a
541 CRISPR/Cas9-mediated approach developed by Zhao et al. with modifications (Zhao *et*
542 *al*, 2017). For gene deletion (deletion of *lacZ* as example), *E. coli* MG1655 was

electrotransformated with pCAGO plasmid which contains both SpCas9 and λ-RED to obtain MG1655-pCAGO. A single colony of the resulting transformant was inoculated into LB medium supplemented with ampicillin (100 mg/ml) and grew overnight at 30°C. 100 μl of the overnight culture was inoculated into 10 ml fresh culture medium and cells were grown at 30°C with IPTG (0.1 mM) induction to OD600 as 0.6. The cells were collected and washed with cold ddH_2O for three times, generating competent cells for electroporation. An aliquot comprising 100 μl competent cells was mixed with 800 ng of the editing-cassette which encompasses 40 bp of sequence among the CDS of *lacZ* gene followed by the chloramphenicol resistant gene, the N20PAM sequence (GTCCATCGAACCGAAGTAAGG), 40 bp upstream-homologous arm of *lacZ* gene, and 40bp downstream-homologous arm of *lacZ* gene, in a 2 mm Gene Pulser cuvette (Bio-Rad) and was subjected to electroporation at 2.3 kV. Following recovering the transformants by cultivation in LB medium for 2 hrs at 30°C, the mixture was spread onto LB agar plate supplemented with ampicillin (100mg/ml), chloramphenicol (25 mg/ml), and 1% glucose (to avoid the background expression of the Cas9 protein). Single colonies were collected and verified by colony PCR to obtain an authentic clone in which the editing-cassette was embedded in chromosomal. The confirmed colony was inoculated into LB medium supplemented with ampicillin (100 mg/ml), IPTG (0.1 mM), and L-arabinose (0.2%) at 30°C overnight to enable expression of SpCas9 and the λ-RED recombinase. The cells were then streaked on LB agar plates supplemented with ampicillin (100mg/ml). Following colony PCR, desired colonies containing deletion of the *lacZ* gene were verified by DNA sequencing (BGI, Shenzhen). For point mutation, (mutation of *pmrB* E36 to A as example) *E. coli* MG1655 was conducted following the same procedures except for the editing cassette sequence which encompasses 40 bp of upstream-homologous arm of GAA (Glu36) followed by the chloramphenicol resistant gene, the N20PAM sequence, the 40 bp upstream-homologous arm of GAA (Glu36), GCA (Ala) and 40 bp downstream-homologous arm of GAA (Glu36). For tag insertion, (insertion 3xFLAG to C-terminal of *arnB* gene as example) *E. coli* MG1655 was conducted following the same procedures except for the editing cassette sequence which

encompasses 40 bp of upstream-homologous arm of stop codon of *arnB* gene followed by the chloramphenicol resistant gene, the N20PAM sequence, the 40 bp upstream-homologous arm of stop codon of *arnB* gene, tag sequence and 40 bp downstream-homologous arm of stop codon of *arnB* gene (include stop codon). After obtaining all desired genome modifications, the editing plasmid was cured by growing the resulting cells at 42°C for 48 hrs.

Construction of pET28A-pBAD-*pmrA* for PmrA protein expression

A DNA fragment encoding the PmrA protein was amplified using genomic DNA of *E. coli* MG1655 as the template and primers specific to this fragment flanked with NcoI and XhoI restriction sites at the 5'- and 3'-end, respectively. After digestion with NcoI and XhoI, and purification using the MiniBEST agarose gel DNA extraction kit (TaKaRa), the purified fragment was ligated into the plasmid pET28a-pBAD and pET28a-pBAD-3xFLAG (Wang *et al.*, 2022) which was treated with the same restriction enzymes using the quick ligation kit (NEB). The resulting construct was selected on LB agar plates supplemented with kanamycin (20 μg/ml) and was verified by DNA sequencing (BGI, Shenzhen). All plasmids constructed are listed in the supplementary Table S4.

Immunoblot analysis

Protein levels of ArnB and PmrA were analyzed by SDS-PAGE following Western Blot. 1ml of cells with OD_{600} of 0.5 was collected and resuspended in 200 μl sample buffer (13 mM Tris, 0.2% SDS, 5% glycerol, 0.004% bromophenol blue, pH 6.8) before being subjected to cell lysis by sonication. Following centrifugation at 13000 rpm for 10 min at 4°C, 20 μl of the sample was separated on SDS-PAGE gels (TGX FastCast Acrylamide Kit, 10%, BIO-RAD). Proteins were then transferred onto a polyvinylidene difluoride (PVDF) membrane (BIO-RAD) using a Trans-Blot SD Semi-Dry Transfer Cell (BioRad) at constant voltage (25 V) for 7 min. Membranes were blocked for 1 h with 5% non-fat milk solution in TBST (20 mM Tris, 150 mM NaCl, 0.1% Tween-20) at room temperature

598 followed by incubation with 1:10,000 primary antibody (monoclonal or polyclonal anti-His
599 antibody) in 1% non-fat milk in TBST at room temperature with shaking for 1 hour. After
600 washing with TBST, the membrane was incubated with the secondary antibody (Goat
601 anti-mouse IgG HRP conjugate) in 1% non-fat milk in TBST at room temperature with
602 shaking for 1 hour. Chemiluminescence of protein bands was detected by ECL Plus
603 Western Blotting Detection Reagents (GE Healthcare, USA), and imaged using a X-ray
604 film development by Alliance Q9 (UVITEC, United Kingdom).

605 **Phos-tag SDS-PAGE**

606 In vivo phosphorylation of PmrA was examined using Phos-Tag SDS-PAGE following our
607 previous description with minor modifications (Wang *et al.*, 2022). *E. coli* MG1655Δ*pmrA*
608 cell harboring pET28a-pBAD-*pmrA*-3×FLAG (AY7068) was inoculated into MOPS
609 minimum medium supplemented with kanamycin (20 μg/ml) and grew overnight at 37°C.
610 100 μl of the overnight culture was inoculated into 5 ml fresh MOPS medium and grew at
611 37°C for 4 hrs. Expression of PmrA was induced with 1mM L-arabinose for 1 hr. Cells
612 were collected by centrifugation at 13000 rpm and were washed with MOPS medium
613 supplemented with 0.1, 0.5, or 1 mM $FeSO_4$ or Pi- MOPS medium twice and shake for 1
614 hr at 37°C in the corresponding medium. 1ml of cells with OD_{600} of 0.5 was collected for
615 the subsequent analysis. Cell pellet was washed with cold PBS twice and was
616 resuspended in 200 μl sample buffer (13 mM Tris, 0.2% SDS, 5% glycerol, 0.004%
617 bromophenol blue, pH 6.8) before being subjected to cell lysis by sonication. Following
618 centrifugation at 13000 rpm for 10 min at 4°C, 20 μl of the sample was loaded onto a 10%
619 Tris-Gly polyacrylamide gel containing 25 mM Phos-tag Acrylamide (Wako) and 50 mM
620 $MnCl_2$. Samples were separated by electrophoresis for 2 hrs at 4°C, following washing
621 with 50 ml transfer buffer containing 10 mM EDTA for 20 min to remove residual Mn^{2+}.
622 Proteins on the gel were transferred onto a PVDF membrane. The membrane was
623 blocked with 5% non-fat milk in TBST buffer and was incubated subsequently with
624 monoclonal ANTI-FLAG® M2 antibody (Sigma) and goat anti-mouse IgG (H+L)-HRP

conjugate (Bio-rad). To detect FLAG-tagged protein bands, the membrane was submerged in the ECL Plus Western Blotting Detection Reagents (GE Healthcare) for 2 min and then subjected to the imaging system (UVITEC Cambridge) to record signals.

Amber codon mutation of selected CouA incorporation sites in pET28A-pBAD-*pmrA*

Selective amino acid located in the DNA binding domain of PmrA was subjected to replacement by CouA, each of these CouA incorporation sites were mutated to a TAG amber codon by site-directed mutagenesis PCR. PCR was conducted using a pair of primers for the desired mutagenesis (Table S3) and pET28A-pBAD-*pmrA* plasmid as the template. PCR product was purified using MiniBEST agarose gel DNA extraction kit (TaKaRa). Following DpnI digestion of the template for 16 hrs, the PCR product was transformed into *E. coli* DH5α. Transformants were recovered on LB agar plates supplemented with kanamycin (20 μg/ml) at 37°C overnight. Colonies recovered were verified by DNA sequencing (BGI, Shenzhen).

In vivo $PmrA_{CouA}$ - $promoter_{SYTO\ 9}$ binding assay

Binding of $PmrA_{CouA}$ and $promoter_{SYTO\ 9}$ was monitored by FRET assay following our previous description with minor modifications (Wang *et al.*, 2022). Plasmid pET28a-pBAD-*pmrA*-G137TAG was co-transformed with pEVOL-CouRS into *E. coli* MG1655 *ΔpmrA* strain, resulting in AY7065 constructs. A fresh single colony of AY7065 was inoculated into MOPS medium supplemented with kanamycin (20 μg/ml) and chloramphenicol (25 μg/ml) and grew overnight at 37°C. 75 μl of the overnight culture was inoculated to 7.5 ml fresh medium to subculture the bacteria. Following culturing at 37°C for 4 hrs, CouA incorporation and expression of PmrA-G137CouA was induced mildly by supplementing 0.9% arabinose and 1mM CouA at 37°C for 5 hrs. Approximately 3.5×10^{10} cells were harvested and washed twice with fresh MOPS medium. Cells were resuspended in MOPS medium as control, or MOPS medium

supplemented with 0.5 mM $FeSO_4$, or Pi- MOPS medium and shake for 1 hr at 37°C. After centrifugation at 4500 rpm for 15 min at 4°C, cell pellet was resuspended in 600 µl of PBS. 85 µl of the suspension was added in each of 6 wells (3 wells for control and 3 wells for experimental group) on a 96-well black plate preloaded with 15 µl of 50 µM SYTO 9 and was incubated for 15 min at room temperature in the dark before being subjected to fluorescence recording (Thermo Scientific Varioskan® Flash spectral scanning multimode reader).

Comparative proteomic analysis

E. coli MG1655 cultured in MOPS medium to OD_{600} of 0.5 was harvested as cells under Pi sufficient condition. The same volume of cells was washed with Pi starvation medium for 3times and resuspended in Pi starvation medium and shake for 3 hrs at 37°C as cells subjected to Pi starvation. Each type of cell pellets with three biological replicates were lysed by resuspending in 20 µl BugBuster reagent (Novagen, USA) (containing 25 mg/ml lysozyme, 1 unit DNase I) at room temperature for 30 mins following centrifugation at 13000 rpm at 4°C for 20 min. Supernatant was transferred to a clean microcentrifuge tube and mixed with 4×SDS sample buffer (40% glycerol, 8% SDS, 240 mM Tris/HCl pH 6.8, 0.04% bromophenol blue) supplemented with 5% β-mercaptoethanol. Sample were incubated at 55 °C for 25 min. 20 µL of each sample were loaded onto a polyacrylamide gel composed of a 10% resolving (lower) gel and a 6% stacking (upper) gel following staining with Coomassie blue staining and fractionated into eight fractions. Gel slices were cut into 1 mm^3 cubes and destained with 50% acetonitrile (ACN) in 50 mm triethyl ammonium bicarbonate (TEAB) and dehydrated with pure CAN and dried in a vacuum concentrator. Sequencing grade modified trypsin (Promega) diluted by an ice-cold buffer containing 50 mM NH4HCO3 and 10% (v/v) ACN was added to cover the dehydrated gel pieces on ice. After 30 min, more trypsin-containing buffer was added to cover the expanded gel pieces followed by overnight incubation at 37 °C. Finally, the resulting tryptic peptides were extracted from the gel by equilibrating the samples with 50% ACN

and 5% formic acid (FA) for 20 min in a 37 °C shaker. The extraction was repeated once, and all fractions were combined and vacuum dried. The protein digest was resuspended in 100 µl of 100 mm TEAB, and then 4 µl of 0.6 m sodium cyanoborohydride ($NaBH_3CN$) were added. Peptides from PI+ and Pi- were labeled with 4 µl of 4% formaldehyde (CH_2O) and deuterated formaldehyde (CD_2O), respectively. The reaction mixture was vortexed and incubated at room temperature for 1 h. The reaction was quenched by sequential addition of 16 µl of 1% (v/v) ammonia solution and 8 µl of formic acid. Finally, light- and heavy-labeled peptides were mixed, and vacuum dried immediately before further mass spectrometric analyses. Extracted peptides were analyzed by Nanoflow LC-MS/MS analyses using the EASY-nLC 1000 System (Thermo Scientific, USA) and LTQ Velos (Thermo Scientific, USA).

Data processing was performed following a previous description (Liu *et al*, 2015). For protein identification, MS/MS spectra were extracted from RAW files using MaxQuant (http://maxquant.org/, version 1.5.3.30). MASCOT (Matrix Science, version 2.3.02) was used to perform database search against an *E. coli* database (strain MG1655, with sequence files downloaded from UniProt in FASTA format, 4,358 entries. Average mass was selected with precursor mass tolerance of 1.5 Da and fragment mass tolerance of 0.8 Da. Methionine oxidation was set as a dynamic modification. The resulting assignments were filtered to achieve a false-discovery rate (FDR) of <1% at both the peptide and protein levels using the target-decoy method. Relative abundances of protein were represented by spectral counts, which are the number of repeated identification of peptides during the entire analysis.

To identify proteins that were differentially expressed in the sets of samples, the spectral counts data were subjected to statistic by DESeq package (Anders and Huber 2010) in R (Team 2014). Briefly, to eliminate the variance caused by sample loading and machine reading depth, the total counts data of two biological conditions was normalized to the same size. The following statistics were performed: *foldChange* (fold change from

condition A to B), *pval* (p value for the statistical significance of this change), and *padj* (p value adjusted for multiple testing with the Benjamini-Hochberg procedure, which controls false discovery rate). Data set with *padj* <0.05 were considered to be significant (Anders and Huber 2010), and corresponding proteins were listed in Table S1.

Polymyxin challenging assay

Challenging *E .coli* cells with designated concentration of polymyxin B (Sigma. USA) were performed as described with modifications (Groisman *et al*, 1997). *E. coli* cells grown under designated conditions were harvested by centrifugation at 13000 rpm for 1min. Cell pellets were re-suspended in MOPS medium to a final concentration of 10^8 cells/ml. The cell culture was treated with polymyxin B with designated concentration for 1-3 hours at 37 °C without agitation. Cell culture prior to and following polymyxin treatment was plated on LB plate, CFU was counted after 12-16 hours incubation at 37°C. Survival of polymyxin challenging was determined by the survival rate of *E. coli* cells after drug treatment. Results are presented as the mean of three biological replicates.

Phylogenetic analysis of EcoPmrB homologs

The PmrB sequences from *E. coli* K-12 MG1655 were used as a query against γ-proteobacteria via BLASTP searches in the UniProt database, with an E-threshold of 10 and the BLOSUM62 substitution matrix. The top 250 retrieved sequences were aligned using the MUSCLE algorithm implemented in MEGA12 software. A phylogenetic tree of EcoPmrB homologous was constructed using the Maximum Likelihood method, with branch support assessed via adaptive bootstrap analysis using 562 bootstrap replicates in MEGA12. The JTT model was applied as the evolutionary model for tree construction.

Statistical analysis

Statistical analysis was performed using GraphPad Prism. Group comparisons between two groups were performed using two-tailed Student's *t* test. Group comparisons between multiple groups were performed using one-way ANOVA or two-way ANOVA with post hoc tests.

Acknowledgments

We thank Ms. Yining Chen in Prof. A. Yan's lab for proofreading the manuscript. We thank Prof. Changhao Bi (Tianjin Institute of Industrial Biotechnology, Chinese Academy of Sciences) for the generous gift of pCAGO plasmid. We thank Prof. Zhaochao Xu and Prof. Lu Miao (CAS Key Laboratory of Separation Science for Analytical Chemistry, Dalian Institute of Chemical Physics, Chinese Academy of Sciences) for the generous gift of OM-sensitive probe PI-BactD. We thank Prof. Patrick C. Y. Woo (Department of Microbiology, University of Hong Kong) for the generous gift of clinical *E. coli* strains.

Funding

This work was supported by the
Research Grants Council of Hong Kong, Theme-based Research Scheme T21-705/20-N (A.Y.)
Research Grants Council of Hong Kong, Collaborative Research Fund C7033-20G (A.Y.)
National Key Research and Development Program of China 2022YFA1304500 (X.L.)
Natural Science Foundation of China 22174003 and 21974002 (X.L.)

Author contributions

G.Z., Z.D., and A.Y. designed research; G.Z., Z.D., J.J., M.W., X.W., X.L., and A.Y. performed research; G.Z., Z.D., X.W., X.L., and A.Y. analyzed data; G.Z., and A.Y. wrote the paper.

Conflicts of interest

Authors declare that they have no competing interests.

Data and materials availability

All data are available in the main text or the supplementary materials.

References

Alves E, Moreirinha C, Faustino MA, Cunha A, Delgadillo I, Neves MG, Almeida A (2016) Overall biochemical changes in bacteria photosensitized with cationic porphyrins monitored by infrared spectroscopy. *Future Medicinal Chemistry* 8: 613-628

Amemura M, Makino K, Shinagawa H, Kobayashi A, Nakata A (1985) Nucleotide sequence of the genes involved in phosphate transport and regulation of the phosphate regulon in *Escherichia coli*. *Journal of molecular biology* 184: 241-250

Bligh EG, Dyer WJ (1959) A rapid method of total lipid extraction and purification. *Canadian journal of biochemistry and physiology* 37: 911-917

Breazeale SD, Ribeiro AA, McClerren AL, Raetz CR (2005) A formyltransferase required for polymyxin resistance in *Escherichia coli* and the modification of lipid A with 4-amino-4-deoxy-L-arabinose: identification and function of UDP-4-deoxy-4-formamido-L-arabinose. *Journal of Biological Chemistry* 280: 14154-14167

Breazeale SD, Ribeiro AA, Raetz CR (2002) Oxidative decarboxylation of UDP-glucuronic acid in extracts of polymyxin-resistant *Escherichia coli*: Origin of lipid a species modified with 4-amino-4-deoxy-l-arabinose. *Journal of Biological Chemistry* 277: 2886-2896

Breazeale SD, Ribeiro AA, Raetz CR (2003) Origin of Lipid A Species Modified with 4-Amino-4-deoxy-l-arabinose in Polymyxin-resistant Mutants of *Escherichia coli*: an aminotransferase (ArnB) that generates UDP-4-amino-4-deoxy-l-arabinose. *Journal of Biological Chemistry* 278: 24731-24739

Breuer W, Epsztejn S, Cabantchik ZI (1995) Iron Acquired from Transferrin by K562 Cells Is Delivered into a Cytoplasmic Pool of Chelatable Iron (II)(∗). *Journal of Biological Chemistry* 270: 24209-24215

Bruna RE, Kendra CG, Groisman EA, Pontes MH (2021) Limitation of phosphate assimilation maintains cytoplasmic magnesium homeostasis. *Proc Natl Acad Sci U S A* 118

Chekabab SM, Harel J, Dozois CM (2014a) Interplay between genetic regulation of phosphate homeostasis and bacterial virulence. *Virulence* 5: 786-793

Chekabab SM, Jubelin G, Dozois CM, Harel J (2014b) PhoB activates *Escherichia coli* O157: H7 virulence factors in response to inorganic phosphate limitation. *PloS one* 9: e94285

Chen HD, Groisman EA (2013) The biology of the PmrA/PmrB two-component system: the major regulator of lipopolysaccharide modifications. *Annual review of microbiology* 67: 83-112

Cheng C, Tennant SM, Azzopardi KI, Bennett-Wood V, Hartland EL, Robins-Browne RM, Tauschek M (2009) Contribution of the *pst-phoU* operon to cell adherence by atypical enteropathogenic *Escherichia coli* and virulence of *Citrobacter rodentium*. *Infection and immunity* 77: 1936-1944

Crépin S, Chekabab S-M, Le Bihan G, Bertrand N, Dozois CM, Harel J (2011) The Pho regulon and the pathogenesis of *Escherichia coli*. *Veterinary microbiology* 153: 82-88

Dahal P (2022) Enterobacteriaceae-definition, characteristics, identification. *Microbe Notes*

Dorrer E, Teuber M (1977) Induction of polymyxin resistance in *Pseudomonas fluorescens* by phosphate limitation. *Archives of Microbiology* 114: 87-89

Eriksson S, Lucchini S, Thompson A, Rhen M, Hinton JC (2003) Unravelling the biology of macrophage infection by gene expression profiling of intracellular *Salmonella enterica*. *Molecular microbiology* 47: 103-118

Fagerbakke KM, Heldal M, Norland S (1996) Content of carbon, nitrogen, oxygen, sulfur and phosphorus in native aquatic and cultured bacteria. *Aquatic Microbial Ecology* 10: 15-27

Fang FC, Frawley ER, Tapscott T, Vázquez-Torres A (2016) Bacterial stress responses during host infection. *Cell host & microbe* 20: 133-143

Feige G, Heinz E, Warge K, Cochems N, Ponzelar E (1980) Discovery of a new glyceroglycolipid in blue-green algae and its role in galactolipid biosynthesis. *Developments in plant biology*

Ferreira GM, Spira B (2008) The pst operon of enteropathogenic *Escherichia coli* enhances bacterial adherence to epithelial cells. *Microbiology* 154: 2025-2036

George TS, Hinsinger P, Turner BL, 2016. Phosphorus in soils and plants–facing phosphorus scarcity. Springer, pp. 1-6.

Gesteland RF (1966) Unfolding of *Escherichia coli* ribosomes by removal of magnesium. *Journal of molecular biology* 18: 356-IN314

Gillooly JF, Allen AP, Brown JH, Elser JJ, Del Rio CM, Savage VM, West GB, Woodruff WH, Woods HA (2005) The metabolic basis of whole-organism RNA and phosphorus content. *Proceedings of the National Academy of Sciences* 102: 11923-11927

Groisman EA, Chiao E, Lipps CJ, Heffron F (1989) *Salmonella* typhimurium *phoP* virulence gene is a transcriptional regulator. *Proceedings of the National Academy of Sciences* 86: 7077-7081

Groisman EA, Kayser J, Soncini FC (1997) Regulation of polymyxin resistance and adaptation to low-Mg^{2+} environments. *Journal of bacteriology* 179: 7040-7045

Gunn JS, Lim KB, Krueger J, Kim K, Guo L, Hackett M, Miller SI (1998) PmrA–PmrB-regulated genes necessary for 4-aminoarabinose lipid A modification and polymyxin resistance. *Molecular microbiology* 27: 1171-1182

Hofstaedter CE, Chandler CE, Met CM, Gillespie JJ, Harro JM, Goodlett DR, Rasko DA, Ernst RK (2024) Divergent Pseudomonas aeruginosa LpxO enzymes perform site-specific lipid A 2-hydroxylation. *Mbio* 15: e02823-02823

Hsieh Y-J, Wanner BL (2010) Global regulation by the seven-component Pi signaling system. *Current opinion in microbiology* 13: 198-203

Huang J, Li C, Song J, Velkov T, Wang L, Zhu Y, Li J (2020) Regulating polymyxin resistance in Gram-negative bacteria: roles of two-component systems PhoPQ and PmrAB. *Future microbiology* 15: 445-459

Jensen V, Löns D, Zaoui C, Bredenbruch F, Meissner A, Dieterich G, Münch R, Häussler S (2006) RhlR expression in *Pseudomonas aeruginosa* is modulated by the *Pseudomonas* quinolone signal via PhoB-dependent and-independent pathways. *Journal of bacteriology* 188: 8601-8606

Jones RA, Shropshire H, Zhao C, Murphy A, Lidbury I, Wei T, Scanlan DJ, Chen Y (2021) Phosphorus stress induces the synthesis of novel glycolipids in *Pseudomonas aeruginosa* that confer protection against a last-resort antibiotic. *ISME J* 15: 3303-3314

Kiriukhin MY, Debabov DV, Shinabarger DL, Neuhaus FC (2001) Biosynthesis of the glycolipid anchor in lipoteichoic acid of *Staphylococcus aureus* RN4220: role of YpfP, the diglucosyldiacylglycerol synthase. *Journal of bacteriology* 183: 3506-3514

Klein DJ, Moore PB, Steitz TA (2004) The contribution of metal ions to the structural stability of the large ribosomal subunit. *Rna* 10: 1366-1379

Lamarche MG, Wanner BL, Crépin S, Harel J (2008) The phosphate regulon and bacterial virulence: a regulatory network connecting phosphate homeostasis and pathogenesis. *FEMS microbiology reviews* 32:

461-473
Lewenza S, Falsafi R, Bains M, Rohs P, Stupak J, Sprott GD, Hancock RE (2011) The *olsA* gene mediates the synthesis of an ornithine lipid in *Pseudomonas aeruginosa* during growth under phosphate-limiting conditions, but is not involved in antimicrobial peptide susceptibility. *FEMS Microbiol Lett* 320: 95-102
Liu Y, Zhang Q, Hu M, Yu K, Fu J, Zhou F, Liu X (2015) Proteomic analyses of intracellular *Salmonella enterica* serovar Typhimurium reveal extensive bacterial adaptations to infected host epithelial cells. *Infection and immunity* 83: 2897-2906
Long S, Miao L, Li R, Deng F, Qiao Q, Liu X, Yan A, Xu Z (2019) Rapid Identification of Bacteria by Membrane-Responsive Aggregation of a Pyrene Derivative. *ACS Sens* 4: 281-285
Makino K, Shinagawa H, Amemura M, Kawamoto T, Yamada M, Nakata A (1989) Signal transduction in the phosphate regulon of *Escherichia coli* involves phosphotransfer between PhoR and PhoB proteins. *Journal of molecular biology* 210: 551-559
Moore C, Mills M, Arrigo K, Berman-Frank I, Bopp L, Boyd P, Galbraith E, Geider R, Guieu C, Jaccard S (2013) Processes and patterns of oceanic nutrient limitation. *Nature geoscience* 6: 701-710
Ogasawara H, Shinohara S, Yamamoto K, Ishihama A (2012) Novel regulation targets of the metal-response BasS-BasR two-component system of *Escherichia coli*. *Microbiology (Reading)* 158: 1482-1492
Olea-Ozuna RJ, Campbell MJ, Quintanilla SY, Nandy S, Brodbelt JS, Boll JM (2025) Alternative lipid synthesis in response to phosphate limitation promotes antibiotic tolerance in Gram-negative ESKAPE pathogens. *PLoS pathogens* 21: e1012933
Perez JC, Groisman EA (2007) Acid pH activation of the PmrA/PmrB two-component regulatory system of *Salmonella enterica*. *Mol Microbiol* 63: 283-293
Perez JC, Shin D, Zwir I, Latifi T, Hadley TJ, Groisman EA (2009) Evolution of a bacterial regulon controlling virulence and Mg^{2+} homeostasis. *PLoS genetics* 5: e1000428
Pontes MH, Groisman EA (2018) Protein synthesis controls phosphate homeostasis. *Genes & development* 32: 79-92
Pontes MH, Sevostyanova A, Groisman EA (2015) When too much ATP is bad for protein synthesis. *Journal of molecular biology* 427: 2586-2594
Poole K (2012) Bacterial stress responses as determinants of antimicrobial resistance. *Journal of Antimicrobial Chemotherapy* 67: 2069-2089
Pratt JT, Ismail AM, Camilli A (2010) PhoB regulates both environmental and virulence gene expression in *Vibrio cholerae*. *Molecular microbiology* 77: 1595-1605
Raetz CR, Reynolds CM, Trent MS, Bishop RE (2007) Lipid A modification systems in gram-negative bacteria. *Annu Rev Biochem* 76: 295-329
Reynolds CM, Raetz CR (2009) Replacement of lipopolysaccharide with free lipid A molecules in *Escherichia coli* mutants lacking all core sugars. *Biochemistry* 48: 9627-9640
Romano S, Schulz-Vogt HN, González JM, Bondarev V (2015) Phosphate limitation induces drastic physiological changes, virulence-related gene expression, and secondary metabolite production in *Pseudovibrio* sp. strain FO-BEG1. *Applied and environmental microbiology* 81: 3518-3528
Romanowski K, Zaborin A, Fernandez H, Poroyko V, Valuckaite V, Gerdes S, Liu DC, Zaborina OY, Alverdy JC (2011) Prevention of siderophore-mediated gut-derived sepsis due to *P. aeruginosa* can be achieved without iron provision by maintaining local phosphate abundance: role of pH. *BMC microbiology* 11: 1-14
Sahonero-Canavesi DX, López-Lara IM, Geiger O (2019) Membrane lipid degradation and lipid cycles in

microbes. *Aerobic Utilization of Hydrocarbons, Oils, and Lipids* 10: 978-973

Santos-Beneit F (2015) The Pho regulon: a huge regulatory network in bacteria. *Frontiers in microbiology* 6: 402

Santos-Beneit F, Martin JF (2013) Vancomycin resistance in *Streptomyces coelicolor* is phosphate-dependent but is not mediated by the PhoP regulator. *J Glob Antimicrob Resist* 1: 109-113

Shinagawa H, Makino K, Nakata A, Brenner S (1983) Regulation of the pho regulon in *Escherichia coli* K-12: genetic and physiological regulation of the positive regulatory gene *phoB*. *Journal of molecular biology* 168: 477-488

Sohlenkamp C, Geiger O (2016) Bacterial membrane lipids: diversity in structures and pathways. *FEMS microbiology reviews* 40: 133-159

Stevenson G, Andrianopoulos K, Hobbs M, Reeves PR (1996) Organization of the *Escherichia coli* K-12 gene cluster responsible for production of the extracellular polysaccharide colanic acid. *Journal of bacteriology* 178: 4885-4893

Stock J, Ninfa A, Stock A (1989) Protein phosphorylation and regulation of adaptive responses in bacteria. *Microbiological reviews* 53: 450-490

Trent MS, Ribeiro AA, Lin S, Cotter RJ, Raetz CR (2001) An Inner Membrane Enzyme in *Salmonella* and *Escherichia coli* That Transfers 4-Amino-4-deoxy-l-arabinose to Lipid A: INDUCTION IN POLYMYXIN-RESISTANT MUTANTS AND ROLE OF A NOVEL LIPID-LINKED DONOR* 210. *Journal of Biological Chemistry* 276: 43122-43131

Van Mooy BA, Fredricks HF, Pedler BE, Dyhrman ST, Karl DM, Koblížek M, Lomas MW, Mincer TJ, Moore LR, Moutin T (2009) Phytoplankton in the ocean use non-phosphorus lipids in response to phosphorus scarcity. *Nature* 458: 69-72

Vences-Guzman MA, Geiger O, Sohlenkamp C (2012) Ornithine lipids and their structural modifications: from A to E and beyond. *FEMS microbiology letters* 335: 1-10

Véscovi EG, Soncini FC, Groisman EA (1996) Mg^{2+} as an extracellular signal: environmental regulation of Salmonella virulence. *Cell* 84: 165-174

Vitousek PM, Porder S, Houlton BZ, Chadwick OA (2010) Terrestrial phosphorus limitation: mechanisms, implications, and nitrogen–phosphorus interactions. *Ecological applications* 20: 5-15

Wang J, Xie J, Schultz PG (2006) A genetically encoded fluorescent amino acid. *Journal of the American Chemical Society* 128: 8738-8739

Wang P, Zhang G, Xu Z, Chen Z, Liu X, Wang C, Zheng C, Wang J, Zhang H, Yan A (2022) Whole-cell FRET monitoring of transcription factor activities enables functional annotation of signal transduction systems in living bacteria. *J Biol Chem*: 102258

Wanner BL (1996) Phosphorus assimilation and control of the phosphate regulon. *Escherichia coli and Salmonella: cellular and molecular biology* 1: 1357-1381

Winfield MD, Groisman EA (2004) Phenotypic differences between *Salmonella* and *Escherichia coli* resulting from the disparate regulation of homologous genes. *Proceedings of the National Academy of Sciences* 101: 17162-17167

Wösten MM, Kox LF, Chamnongpol S, Soncini FC, Groisman EA (2000) A signal transduction system that responds to extracellular iron. *Cell* 103: 113-125

Xu Z, Wang P, Wang H, Yu ZH, Au-Yeung HY, Hirayama T, Sun H, Yan A (2019) Zinc excess increases cellular demand for iron and decreases tolerance to copper in *Escherichia coli*. *J Biol Chem* 294: 16978-16991

Yan A, Guan Z, Raetz CR (2007) An undecaprenyl phosphate-aminoarabinose flippase required for polymyxin resistance in *Escherichia coli*. *J Biol Chem* 282: 36077-36089

Zhao D, Feng X, Zhu X, Wu T, Zhang X, Bi C (2017) CRISPR/Cas9-assisted gRNA-free one-step genome editing with no sequence limitations and improved targeting efficiency. *Sci Rep* 7: 16624

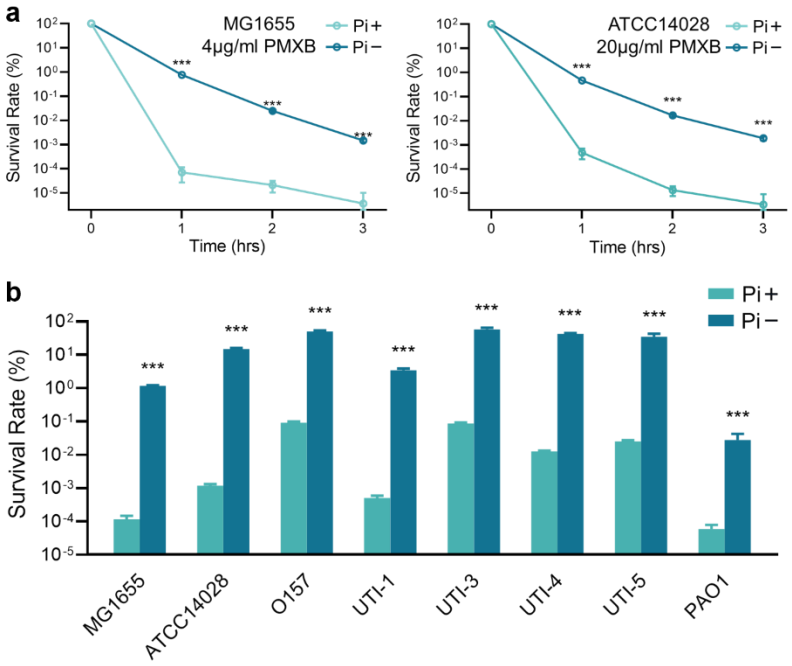

Figure 1. Pi starvation induced polymyxin resistance in *Enterobacteriaceae*. (**A**) Survival of *E. coli* MG1655 and *S.* Typhimurium ATCC14028 with or without Pi starvation treatment against polymyxin B for 3 hrs (4 μg/ml for *E. coli* and 20 μg/ml for *S.* Typhimurium). (**B**) Survival rates of *E. coli* MG1655, *S.* Typhimurium ATCC14028, pathogenic *E. coli* O157, UTI-1, UTI-3, UTI-4, UTI-5, and *P. aeruginosa* PAO1 with or without Pi starvation for 3 hrs against polymyxin B (4 μg/ml for *E. coli* strains, 20 μg/ml for *S.* Typhimurium and 8 μg/ml for *P. aeruginosa*) for 1 hr. Data are presented as mean ± s.d. of three biological replicates. Statistical significance was assessed using two-tailed Student's t-test. Significance levels are indicated as follows: *$p < 0.05$; **$p < 0.01$; ***$p < 0.001$.

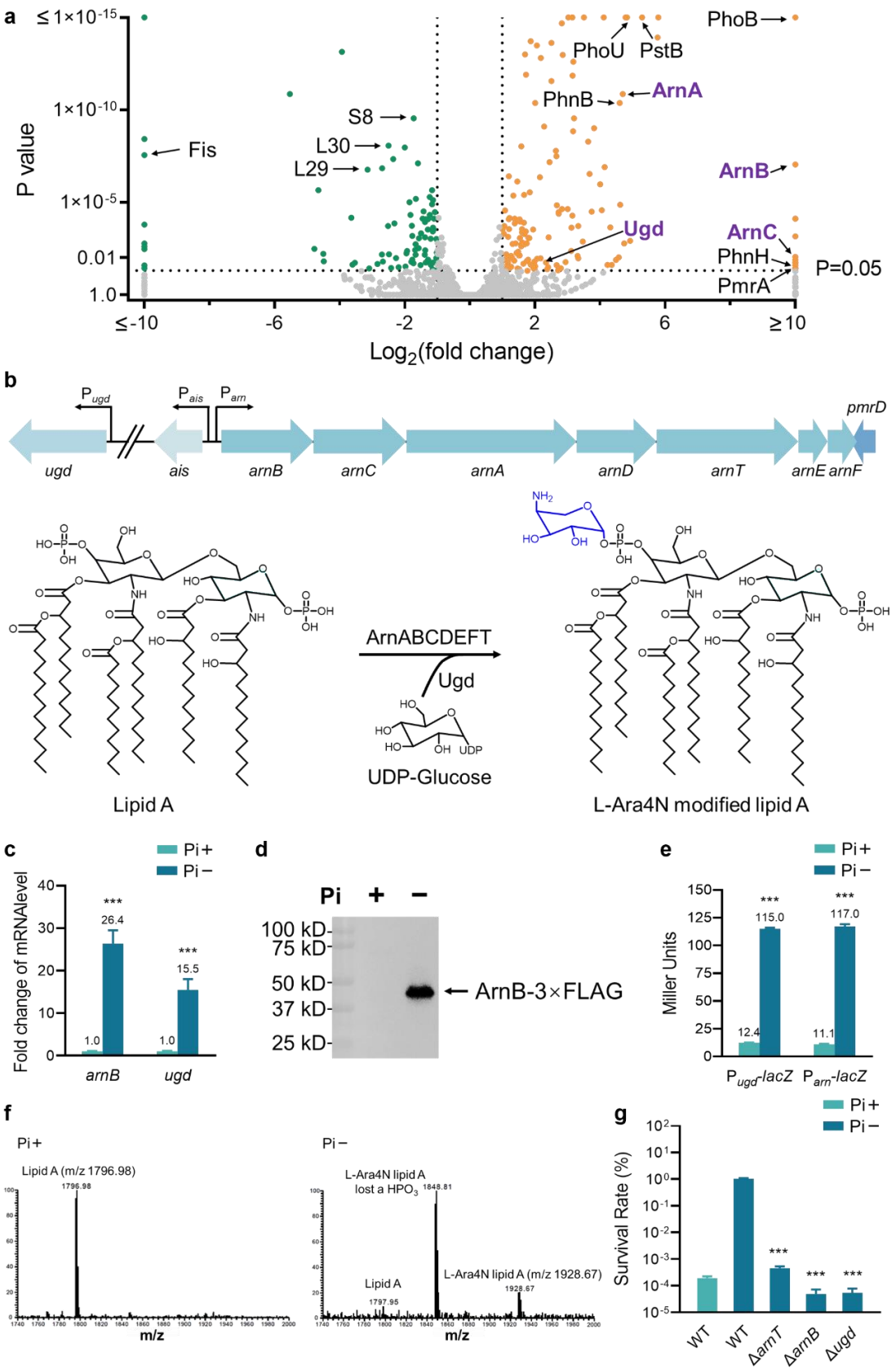

Figure 2. Pi starvation induced the expression of *ugd-arn* system to modify lipid A

with L-Ara-4N, conferring stress-induced polymyxin resistance.
(**A**) Volcano plot depicting differentially expressed proteins following 3 hours incubation in Pi starvation condition relative to Pi-sufficient conditions. Red (right) and blue (left) dots represent significantly up-regulated and down-regulated proteins, respectively. The horizontal dashed line depicts a p-value cutoff (0.05), and vertical dashed lines depict 1/2 and 2-fold ratio cutoffs. Selected proteins are labeled. (**B**) Genetic organization of the *arn* operon and *ugd* gene in MG1655. Ugd and ArnABCDEFT catalyze the biosynthesis of 4-amino-4-deoxy-L-arabinose (L-Ara4N) and its modification of lipid A. (**C**) mRNA levels of *ugd* and *arnB* under Pi-sufficient and Pi-starvation conditions detected by RT-qPCR. (**D**) Production of ArnB-3×FLAG under Pi-sufficient and Pi-starvation conditions detected by Western blot. The protein band corresponding to ArnB-3×FLAG is marked. (**E**) β-galactosidase activities of P_{arn}-*lacZ* and P_{ugd}-*lacZ* in MG1655 Δ*lacZ* under Pi-sufficient and Pi-starvation conditions. (**F**) ESI-MS spectra of lipid A molecules extracted from *E. coli* MG1655 cells cultured under Pi sufficient (left) and subjected to Pi starvation conditions (right). Peaks corresponding to native lipid A and L-Ara-4N modified lipid A were shown. (**G**) Survival of *E. coli* MG1655 parent and isogenic Δ*arnT*, Δ*arnB* and Δ*ugd* mutants following Pi starvation treatment for 3 hrs against 4 μg/ml polymyxin B for 1 hr. Data are presented as mean ± s.d. of three biological replicates for **C**, **E**, and **G**. Statistical significance was assessed using two-tailed Student's t-test for **C** and **E**, and one-way ANOVA followed by Dunnett's multiple comparisons test for **G**. Significance levels are indicated as follows: $^{*}p < 0.05$; $^{**}p < 0.01$; $^{***}p < 0.001$.

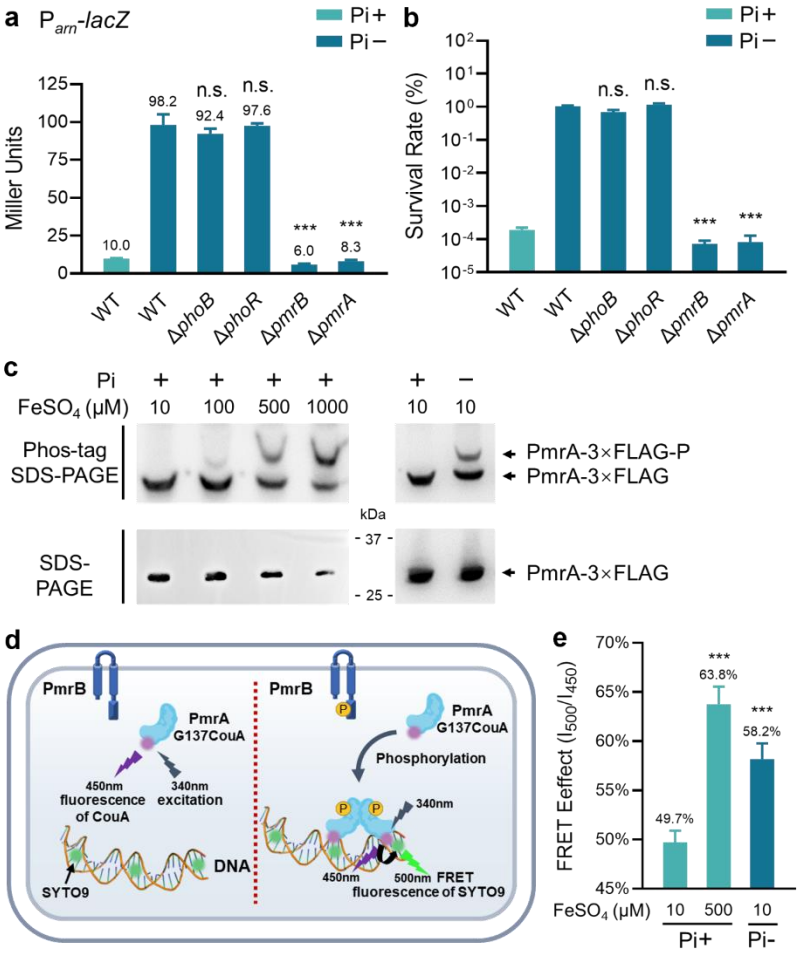

Figure 3. The PmrAB two-component system is activated during Pi starvation and is responsible for the up-regulation of *arn* and *ugd* genes under this condition. (**A**) β-galactosidase activities of P_{arn}-*lacZ* in MG1655 Δ*lacZ* parent and isogenic Δ*pmrB*, Δ*pmrA,* Δ*phoB,* and Δ*phoR* mutants under conditions depicted. (**B**) Survival of *E. coli* MG1655 parent and isogenic Δ*pmrB*, Δ*pmrA,* Δ*phoB,* and Δ*phoR* mutants following Pi starvation treatment for 3 hrs against 4 μg/ml polymyxin B for 1 hr. (**C**) Phosphorylation of PmrA-3×FLAG detected by Phos-Tag SDS–PAGE following immunoblotting with anti-FLAG antibody under the indicated culture conditions. Protein bands representing PmrA-3×FLAG and PmrA-3×FLAG-P are indicated. (**D**) Schematic diagram of the whole-cell FRET measurement of PmrA-promoter binding assay. A bright fluorescent unnatural amino acid donor CouA (red spheres) is incorporated into G137 of PmrA in DNA-binding domain. SYTO9 (green spheres) is employed to stain chromosome DNA in living *E. coli* MG1655. (**E**) Quantification of the FRET effect between the CouA-SYTO9 pair in *E. coli* cells treated with iron excess under Pi sufficient condition and Pi starvation condition without Fe excess. Data are presented as mean ± s.d. of three biological replicates for **A**, **B**, and **E**. Statistical significance was assessed using one-way ANOVA followed by Dunnett's multiple comparisons test for **A**, **B**, and **E**. Significance levels are indicated as follows: *$p < 0.05$; **$p < 0.01$; ***$p < 0.001$.

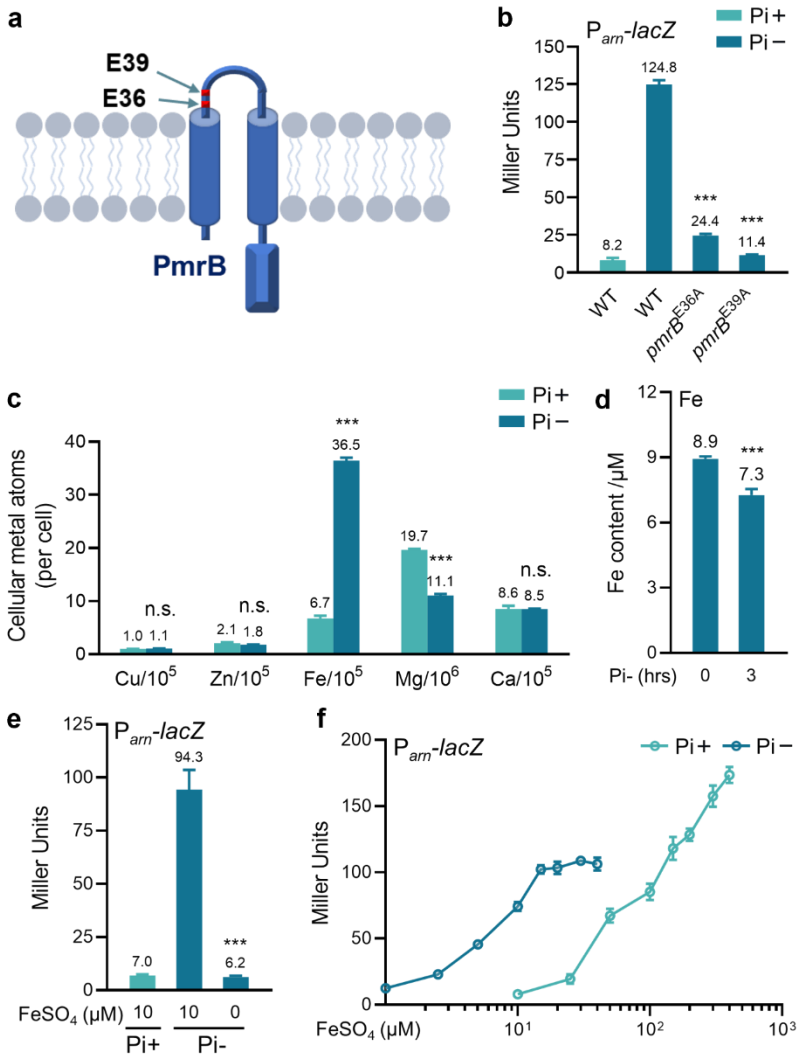

Figure 4. Activation of PmrAB during Pi starvation is mediated by the secondary stress signal iron (Fe^{3+}) induced under this condition

(**A**) Schematic diagram of the sensor kinase PmrB. Two important residues for sensing Fe^{3+}, E36A and E39A, are shown. (**B**) β-galactosidase activities of P_{arn}-*lacZ* in MG1655 Δ*lacZ* parent and isogenic *pmrB*^{E36A} and *pmrB*^{E36A} mutants under Pi sufficient and Pi starvation conditions. (**C**) Cellular metal contents in *E. coli* MG1655 under Pi sufficient and Pi starvation conditions determined by ICP-MS. (**D**) Iron contents in the spent medium of *E. coli* MG1655 following Pi-depletion at the indicated time points. (**E**) β-galactosidase activities of P_{arn}-*lacZ* in MG1655 Δ*lacZ* in Pi sufficient, Pi-depleted, and Fe-free Pi-depleted culture conditions. (**F**) β-galactosidase activities of P_{arn}-*lacZ* in MG1655 Δ*lacZ* under Pi sufficient and Pi starvation conditions in the presence of different concentrations of $FeSO_4$. Data are presented as mean ± s.d. of three biological replicates for **B**, **C**, **D**, **E**, and **F**. Statistical significance was assessed using one-way ANOVA followed by Dunnett's multiple comparisons test for **B**, and two-tailed Student's t-test for **C**, **D**, and **E**. Significance levels are indicated as follows: $*p < 0.05$; $**p < 0.01$; $***p < 0.001$.

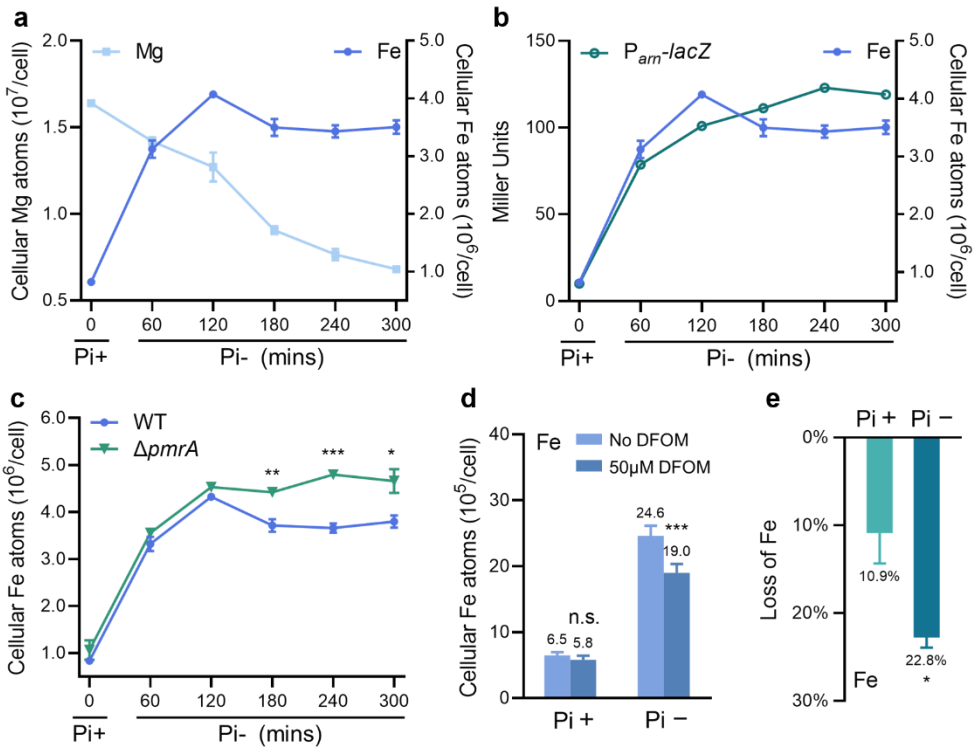

Figure 5. Response to Pi starvation induced iron mobilization to cell surfaces

(**A**) Iron (Fe) and magnesium (Mg) contents in *E. coli* MG1655 subjected to Pi-depleted medium at the indicated time points. (**B**) β-galactosidase activities of P_{arn}-*lacZ* in MG1655 Δ*lacZ* and Fe contents in *E. coli* MG1655 subjected to Pi-depleted medium at the indicated time points. (**C**) Fe contents in *E. coli* MG1655 parent and isogenic Δ*pmrA* mutant subjected to Pi-depleted medium at the indicated time points. (**D**) Fe contents in *E. coli* MG1655 under Pi sufficient and Pi starvation conditions following washing by HEPES or DFOM-supplemented (50μM) HEPES buffer. (**E**) Reduction of cellular Fe content following washing with DFOM-supplemented HEPES buffer. Data are presented as mean ± s.d. of three biological replicates. Statistical significance was assessed using two-tailed Student's t-test for **C** and **E**, and two-way ANOVA followed by Sidak's multiple comparisons test for **D**. Significance levels are indicated as follows: *$p < 0.05$; **$p < 0.01$; ***$p < 0.001$.

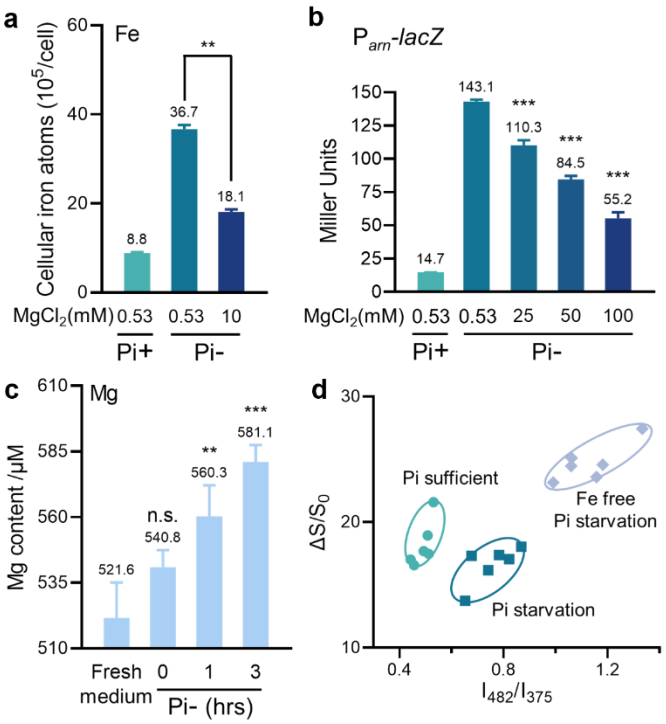

Figure 6. Iron mobilization is driven by Mg^{2+} dissociation during Pi starvation

(**A**) Fe contents in *E. coli* MG1655 under Pi sufficient and Pi starvation conditions supplemented with various concentration of $MgCl_2$. (**B**) β-galactosidase activities of P_{arn}-*lacZ* in MG1655 Δ*lacZ* under Pi sufficient and Pi starvation conditions supplemented with different concentration of $MgCl_2$. (**C**) Mg content in the spent medium of *E. coli* MG1655 subjected to Pi-depleted medium at the indicated time points. (**D**) 2D graph plotted from output signals of two channels of the PI-BactD sensor: fluorescence increase (ΔS/S0) and fluorescence radiometric changes (I482/I375) in each of the treatments indicated. Data are presented as mean ± s.d. of three biological replicates for **A**, **B**, and **C**, and six biological replicates for **D**. Statistical significance was assessed using two-tailed Student's t-test for **a**, and one-way ANOVA followed by Dunnett's multiple comparisons test for **B** and **C**. Significance levels are indicated as follows: $*p < 0.05$; $**p < 0.01$; $***p < 0.001$.

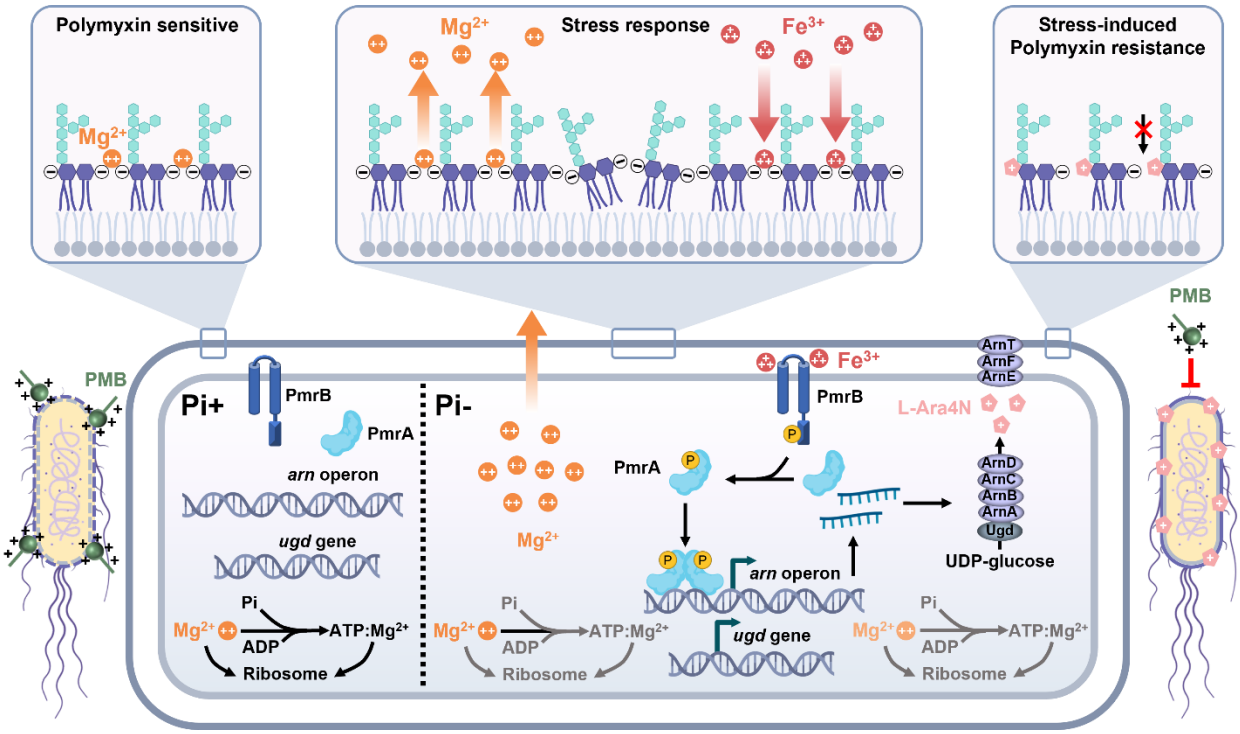

Figure 7. A Mg-Fe-PmrAB regulatory circuit underpins the Pi-starvation induced polymyxin resistance through activating the lipid A L-Ara4N modification system

In Pi sufficient cultures, ribosome and ATP serve as the major intracellular Mg^{2+} and Pi reservoir. Mg^{2+} neutralizes negative charge of lipid A and stabilizes outer membrane (OM). The PmrAB two-component system (TCS) is inactive, and the cell is sensitive to polymyxin. During Pi starvation, ATP biosynthesis and ribosome biogenesis are halted due to Pi depletion, disrupting the balance between Pi and Mg^{2+}. Mg^{2+} disassociates from the cell which destabilizes the OM and derives compensatory Fe^{3+} mobilization to cell surface. Mobilized Fe^{3+} activates the PmrAB TCS which in turn upregulates the *arn* operon. Arn and Ugd proteins catalyze the biosynthesis of L-Arn4N and modify lipid A with L-Arn4N to stabilize OM under stressed condition and prevent further Fe mobilization. *E. coli* cells with L-Arn4N modified lipid A become resistant to polymyxin.

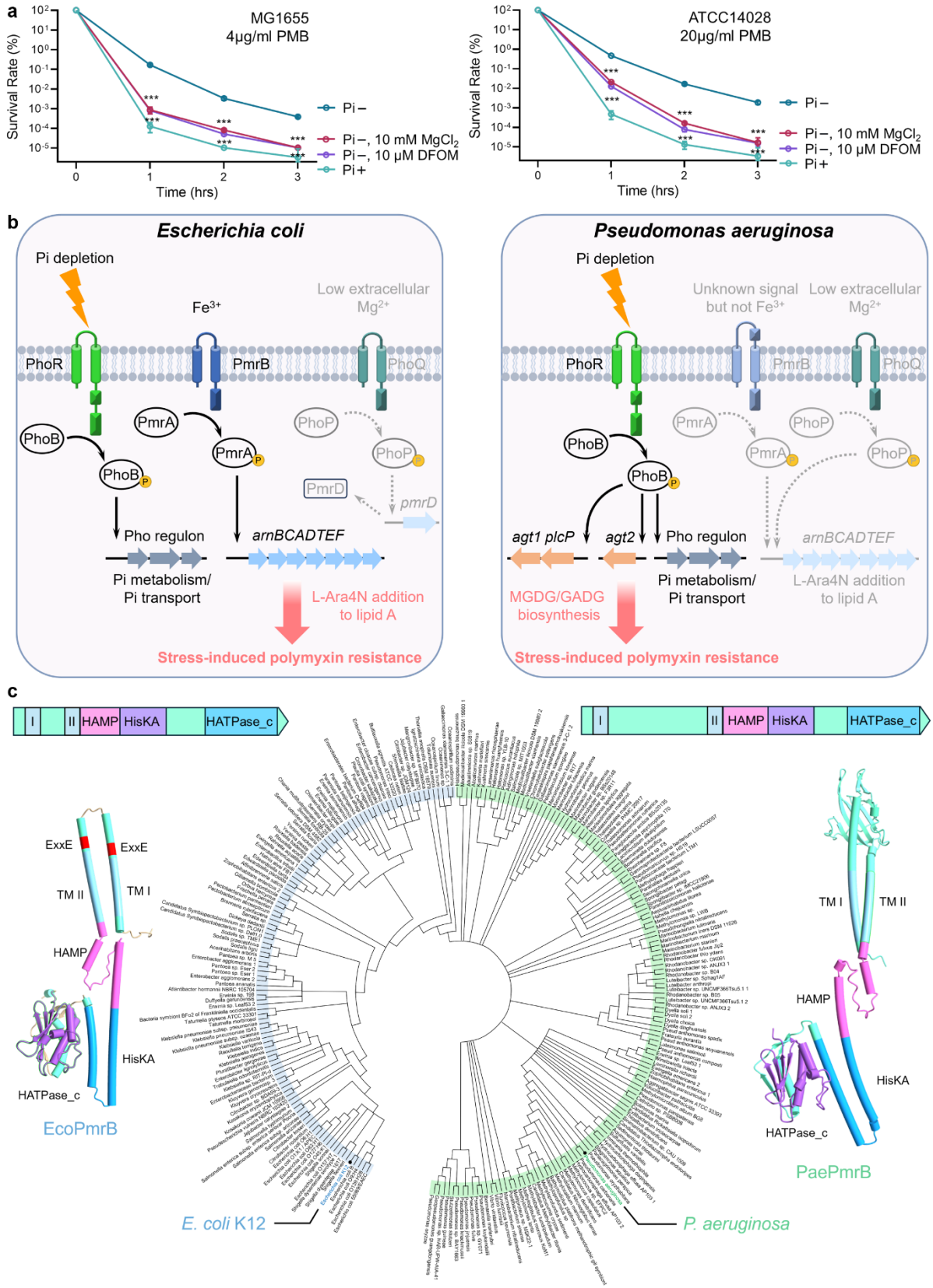

Figure 8. Disrupting the Mg-Fe-PmrAB signaling circuit abolished Pi-starvation induced polymyxin resistance in *Enterobacteriaceae*

(**A**) Survival of *E. coli* MG1655 cells and *S.* Typhimurium ATCC14028 cells with or without Pi starvation treatment supplemented with10mM $MgCl_2$ or 10 μM DFOM against 4 μg/ml and 20 μg/ml polymyxin B for 3 hrs. (**B**) Distinct stress adaptation strategies in *E. coli* and *P. aeruginosa* under Pi starvation conditions. Genes and regulatory systems activated in the two species are illustrated. Inactive regulatory systems are depicted in faded effects. The regulatory mechanisms for *P. aeruginosa* are based on findings from Jones et. al (Jones *et al.*, 2021). (**C**) A phylogenetic tree of 250 PmrB homologous. A predominant clade is indicated by a blue circle, comprising sequences from bacteria such as *Escherichia, Shigella, Citrobacter, Salmonella, Klebsiella, Yersinia*, and *Enterobacter* species. A green circle marks several clades distinct from the predominant one. The domain architecture and AlphaFold3-predicted structure of EcoPmrB and PaePmrB are shown. Data are presented as mean ± s.d. of three biological replicates for **A**. Statistical significance was assessed using one-way ANOVA followed by Dunnett's multiple comparisons test. Significance levels are indicated as follows: $*p < 0.05$; $**p < 0.01$; $***p < 0.001$.

Expanded View Figures

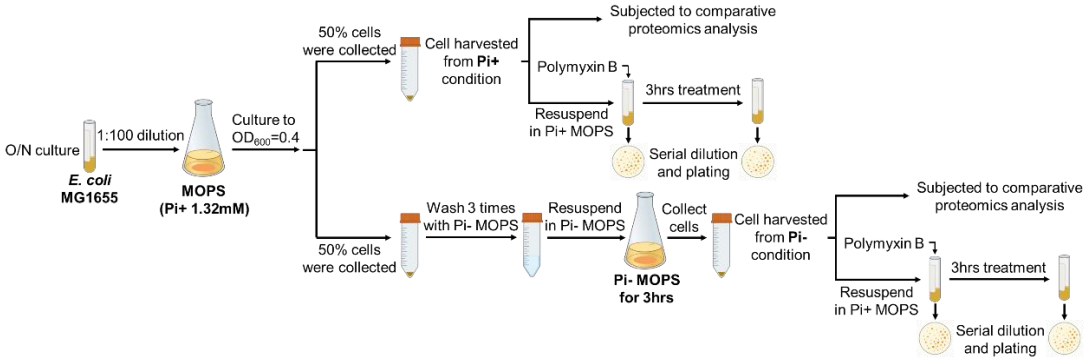

Figure EV1. Workflow of acute Pi starvation treatment and following proteomic sample preparation and polymyxin B challenging assay.
Bacteria were cultured to an OD_{600} of 0.4 in standard MOPS synthetic medium containing 1.32 mM inorganic phosphate (Pi), representing Pi-sufficient conditions. For Pi-starvation conditions, bacteria were first grown to OD_{600} = 0.4 in the same medium, then transferred to Pi-depleted MOPS medium (0 mM Pi). For comparative proteomic analysis, the collected bacterial cells were subjected to sample preparation and proteomic analysis. For the polymyxin challenging assay, the collected bacterial cells were resuspended in standard MOPS medium and treated with the designated concentration of polymyxin B. Cell viability was assessed at the beginning and end of treatment by serial dilution and plating.

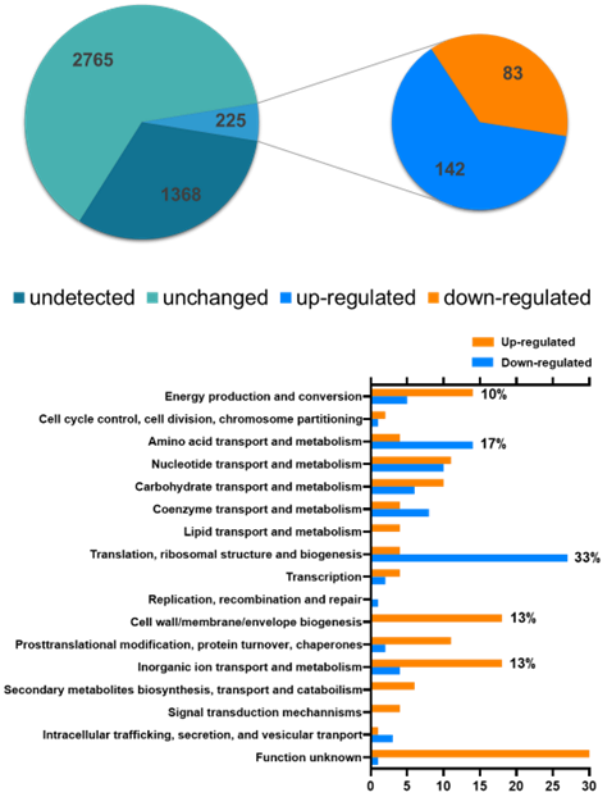

Figure EV2. Quantitative proteomic analysis of *E. coli* MG1655 in response to acute Pi starvation.

Pie chart of total and differentially expressed proteins detected by LC-MS/MS analysis in *E. coli* MG1655 cells subjected to Pi starvation for 3 hours, relative to cells under Pi sufficient conditions. Red and blue colors represent significantly upregulated and downregulated proteins, respectively. Clusters of Orthologous Groups (COG) functional categories of differentially expressed proteins in *E. coli* MG1655 in response to Pi starvation. Red and blue colors represent significantly upregulated and downregulated proteins, respectively.

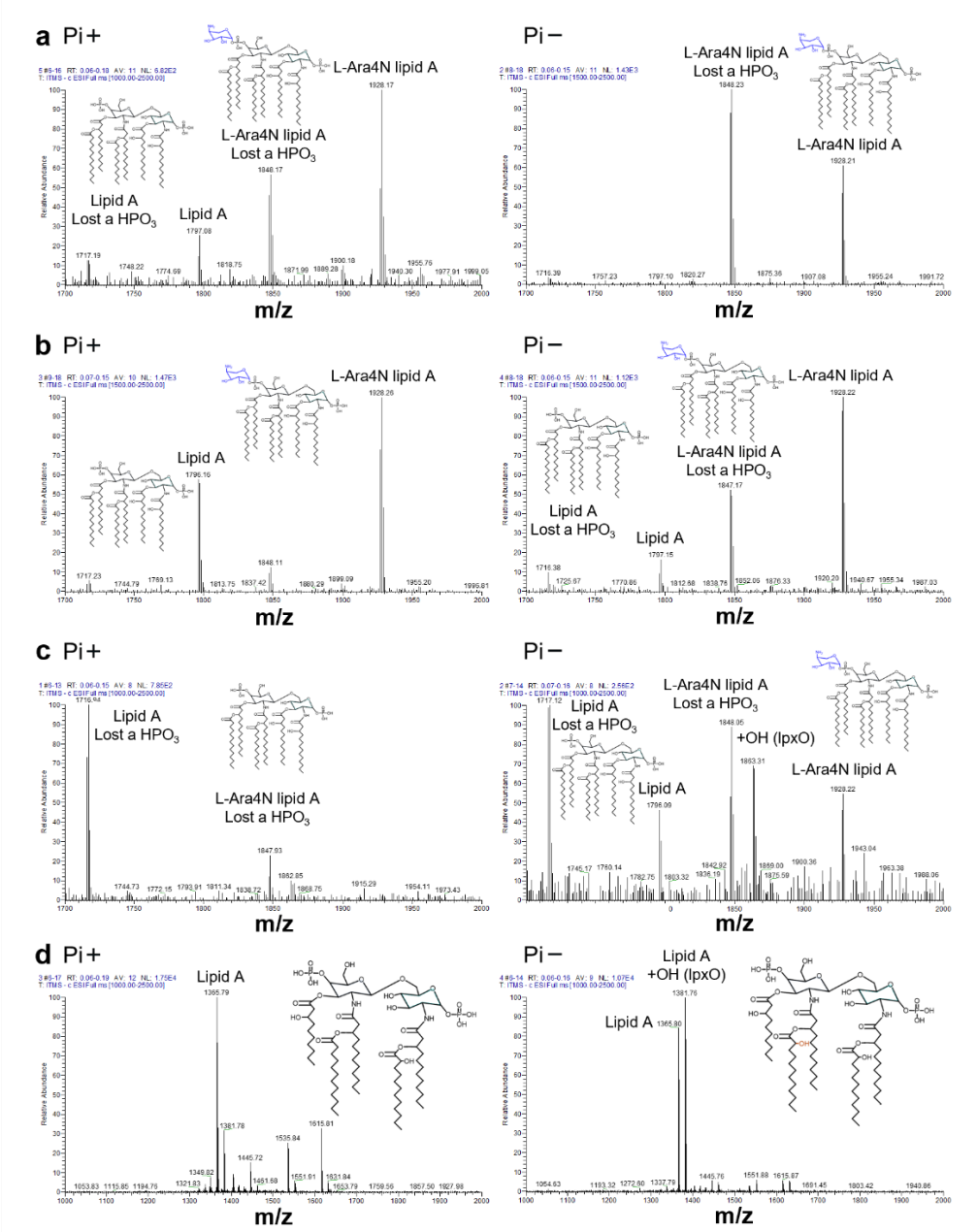

Figure EV3. The ratio of L-Ara-4N modified Lipid A molecule increases in *E. coli* O157, *E. coli* UTI-3, *S.* Typhimurium ATCC14028 and *P. aeruginosa* PAO1 cells subjected to Pi starvation.

(**A**) ESI-MS spectra of lipid A molecules extracted from *E. coli* O157 cells cultured under Pi sufficient (left) and subjected to Pi starvation conditions (right). Peaks correspond to native lipid A and L-Ara-4N modified lipid A are shown. (**B**) ESI-MS spectra of lipid A molecules extracted from *E. coli* UTI-3 cells cultured under Pi sufficient (left) and subjected to Pi starvation conditions (right). Peaks correspond to native lipid A and L-Ara-4N modified lipid A are shown. (**C**) ESI-MS spectra of lipid A molecules extracted from *S.* Typhimurium ATCC14028 cells cultured under Pi sufficient (left) and subjected to Pi starvation conditions (right). Peaks correspond to native lipid A and modified lipid A are shown. (**D**) ESI-MS spectra of lipid A molecules extracted from PAO1 cells cultured under

Pi sufficient (left) and subjected to Pi starvation conditions (right). Peaks correspond to native lipid A and modified lipid A are shown.

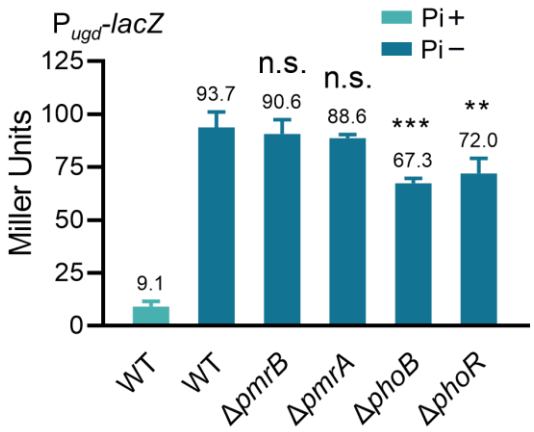

Figure EV4. Up-regulation of *ugd* gene during Pi starvation is independent of PmrAB TCS, but partially dependent on PhoBR TCS in *E. coli* MG1655.
β-galactosidase activities of P_{ugd}-*lacZ* in MG1655 Δ*lacZ* parent and isogenic Δ*pmrB,* Δ*pmrA,* Δ*phoB* and Δ*phoR* mutants under Pi sufficient and Pi starvation conditions. Data are presented as mean ± s.d. of three biological replicates. Statistical significance was assessed using one-way ANOVA followed by Dunnett's multiple comparisons test. Significance levels are indicated as follows: *$p < 0.05$; **$p < 0.01$; ***$p < 0.001$.

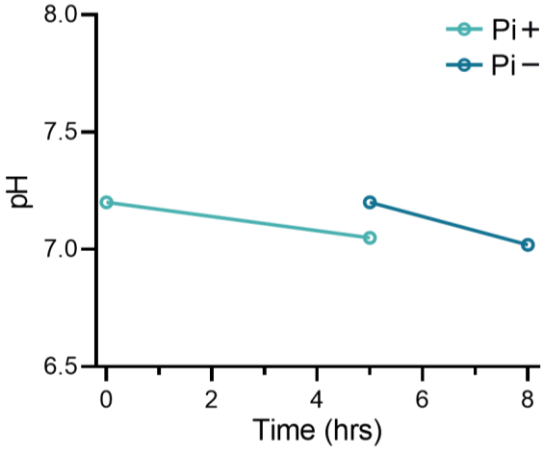

Figure EV5. pH of spent medium of *E. coli* MG1655 after 5hrs Pi sufficient growth and after 3hrs Pi starvation treatment.

pH of the medium before bacteria inoculating and pH of the spent medium after 5hrs Pi sufficient growth or 3hrs Pi starvation treatment were measured. Data are presented as mean ± s.d. of three biological replicates.

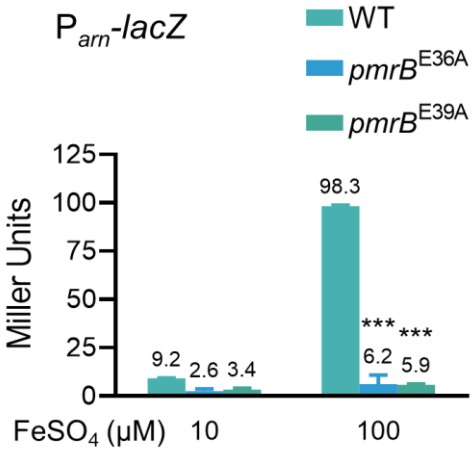

Figure EV6. E36A and E39A mutation abolish the Fe^{3+} signaling capacity of PmrA. β-galactosidase activities of P_{arn}-*lacZ* in MG1655 Δ*lacZ* parent and isogenic *pmrB*^{E36A}, *pmrB*^{E39A} mutants under Pi sufficient conditions supplemented with different concentration of $FeSO_4$. Data are presented as mean ± s.d. of three biological replicates. Statistical significance was assessed using two-way ANOVA followed by Dunnett's multiple comparisons test. Significance levels are indicated as follows: *$p < 0.05$; **$p < 0.01$; ***$p < 0.001$.

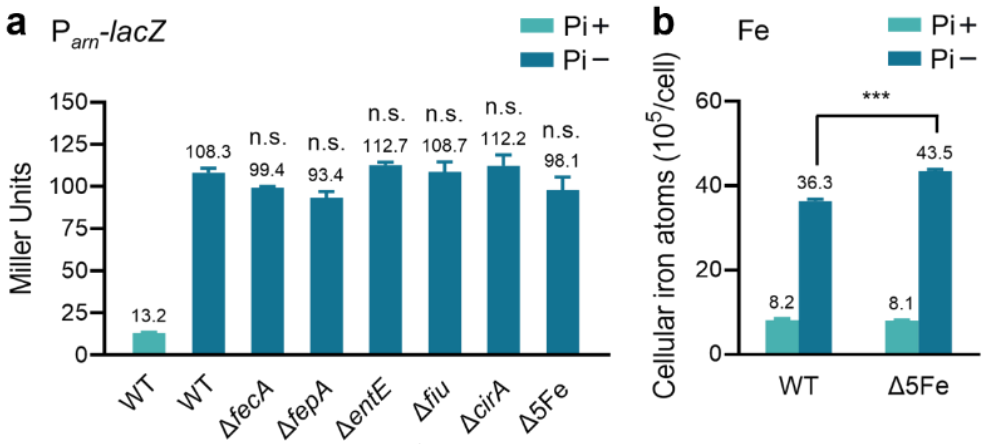

Figure EV7. Deletion of canonical Fe^{3+} up-take genes does not affect the activation of PmrAB system and increase of Fe mobilization to *E. coli* cell during Pi starvation.

(**A**) β-galactosidase activities of P_{arn}-*lacZ* in MG1655 Δ*lacZ* parent and isogenic Δ*fecA*, Δ*fepA*, Δ*entE*, Δ*fiu*, Δ*cirA*, and Δ5Fe (Δ*fecA*Δ*fepA*Δ*entE*Δ*fiu*Δ*cirA*) mutants under Pi sufficient and Pi starvation conditions. (**B**) Fe contents in *E. coli* MG1655 parent and isogenic Δ*fecA* Δ*fepA* Δ*entE* Δ*fiu* Δ*cirA* mutant under Pi sufficient and Pi starvation conditions. Data are presented as mean ± s.d. of three biological replicates. Statistical significance was assessed using one-way ANOVA followed by Dunnett's multiple comparisons test for **A** and two-way ANOVA followed by Sidak's multiple comparisons test for **B**. Significance levels are indicated as follows: *$p < 0.05$; **$p < 0.01$; ***$p < 0.001$.

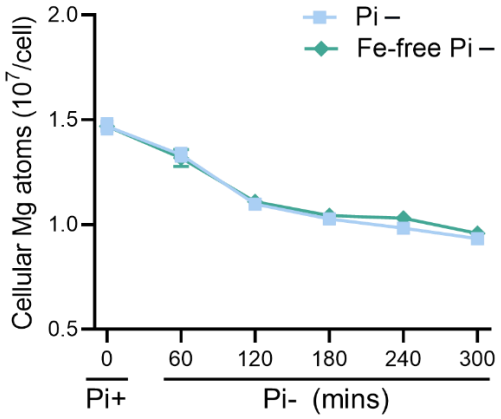

Figure EV8. Decrease of cellular magnesium during Pi starvation was independent of Fe from medium.

Mg contents in *E. coli* MG1655 subjected to Pi-depleted medium or Fe-free Pi-depleted medium at the indicated time points. Data are presented as mean ± s.d. of three biological replicates.

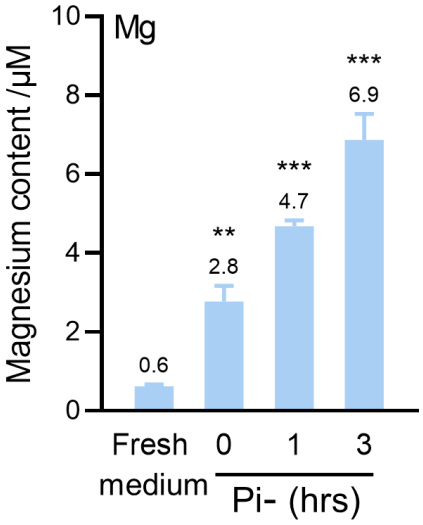

Figure EV9. Magnesium disassociates from *E. coli* cells when subjected to Mg-free Pi-depleted medium.

Mg content in the spent medium of *E. coli* MG1655 subjected to Mg-free Pi-depleted medium at the indicated time points. Data are presented as mean ± s.d. of three biological replicates. Statistical significance was assessed using one-way ANOVA followed by Dunnett's multiple comparisons test. Significance levels are indicated as follows: *$p < 0.05$; **$p < 0.01$; ***$p < 0.001$.

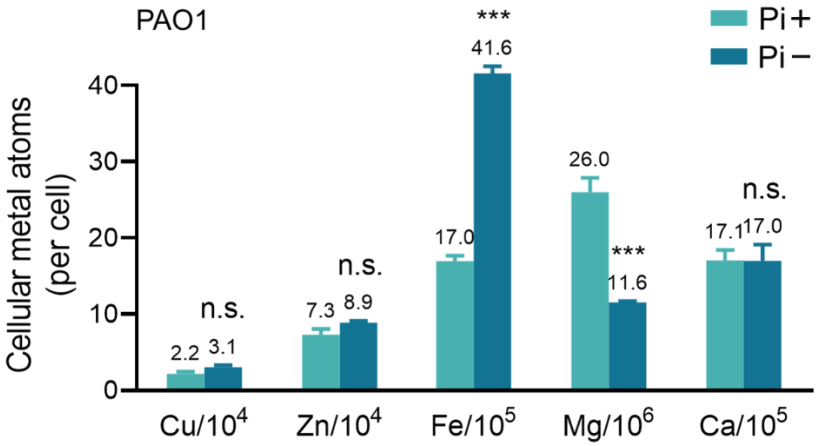

Figure EV10. Cellular metal content in *P. aeruginosa* PAO1 cells collected from Pi-sufficient cultures or subjected to Pi-depletion treatment.

Cellular metal contents in *P. aeruginosa* PAO1 under Pi sufficient and Pi starvation conditions determined by ICP-MS. Data are presented as mean ± s.d. of three biological replicates. Statistical significance was assessed using two-tailed Student's t-test. Significance levels are indicated as follows: *$p < 0.05$; **$p < 0.01$; ***$p < 0.001$.

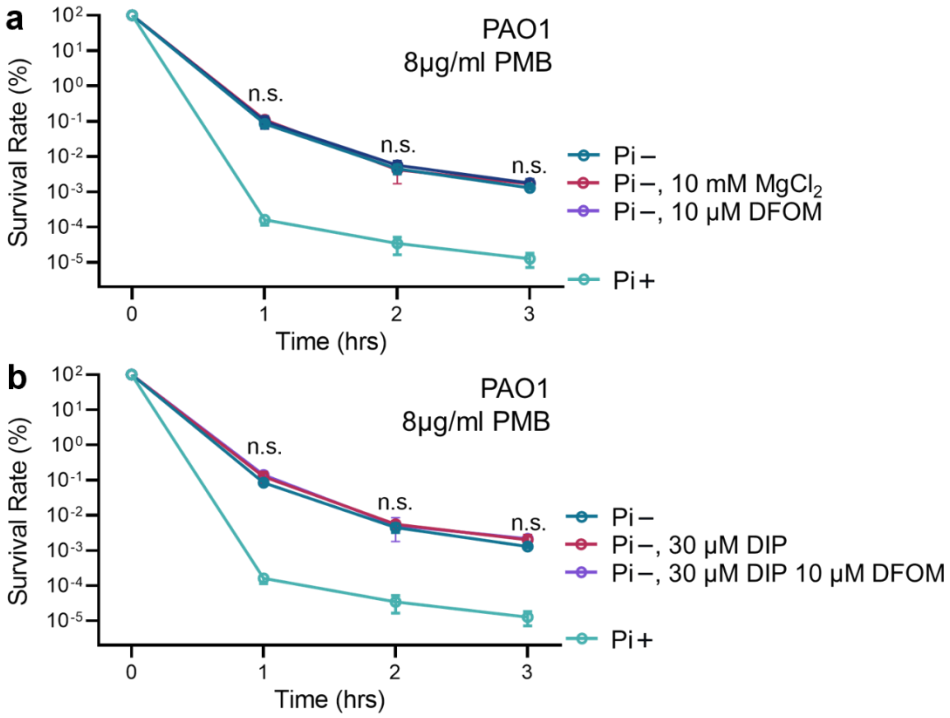

Figure EV11. Disruption of Mg and Fe signaling showed no effect on Pi-starvation induced polymyxin resistance in *P. aeruginosa.*

(A) Survival of *P. aeruginosa* PAO1 cells with or without Pi starvation treatment supplemented with10mM $MgCl_2$ or 10 μM DFOM against 20 μg/ml polymyxin B for 3 hrs. (B) Survival of *P. aeruginosa* PAO1 cells with or without Pi starvation treatment supplemented with 30 μM DIP or 30 μM DIP and 10 μM DFOM against 20 μg/ml polymyxin B for 3 hrs. Data are presented as mean ± s.d. of three biological replicates. Statistical significance was assessed using one-way ANOVA followed by Dunnett's multiple comparisons test. Significance levels are indicated as follows: $*p < 0.05$; $**p < 0.01$; $***p < 0.001$.

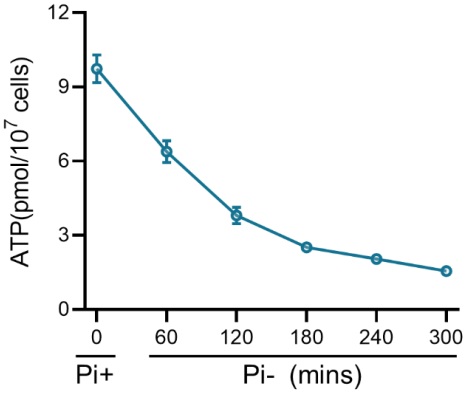

Figure EV12. Cellular ATP level in *E. coli* MG1655 cells continuously decrease during Pi starvation.

Cellular ATP levels in *E. coli* MG1655 subjected to Pi-depleted medium at the specified time points. Data are presented as mean ± s.d. of three biological replicates.

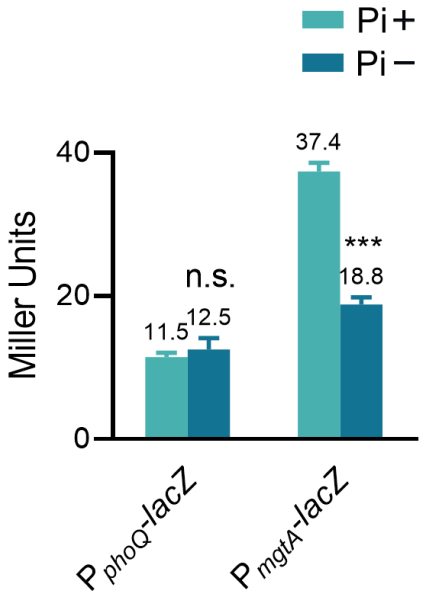

Figure EV13. Lack of upregulation of *phoQ* and *mgtA* genes indicates that the PhoPQ TCS is not activated during Pi starvation in *E. coli* MG1655.
β-galactosidase activities of P_{phoQ}-*lacZ* and P_{mgtA}-*lacZ* in MG1655 Δ*lacZ* parent under Pi sufficient and Pi starvation conditions. Data are presented as mean ± s.d. of three biological replicates for A. Statistical significance was assessed using two-tailed Student's t-test. Significance levels are indicated as follows: *$p < 0.05$; **$p < 0.01$; ***$p < 0.001$.

Supplementary tables

Table S1. Proteins identified to be different expressed in *E. coli* MG1655 growing under Pi sufficient and starvation conditions

prot_desc	id	log2FoldChange	padj
argF	sp|P06960|OTC2_ECOLI	-Inf	3.42E-18
gatZ	sp|P0C8J8|GATZ_ECOLI	-Inf	3.77E-09
fis	sp|P0A6R3|FIS_ECOLI	-Inf	2.78E-08
secY	sp|P0AGA2|SECY_ECOLI	-Inf	0.000159211
kgtP	sp|P0AEX3|KGTP_ECOLI	-Inf	0.001647533
gatC	sp|P69831|PTKC_ECOLI	-Inf	0.002435201
cysC	sp|P0A6J1|CYSC_ECOLI	-Inf	0.003341414
znuC	sp|P0A9X1|ZNUC_ECOLI	-Inf	0.025826417
rffH	sp|P61887|RMLA2_ECOLI	-Inf	0.036760697
cysD	sp|P21156|CYSD_ECOLI	-5.525585778	1.38E-11
mnmG	sp|P0A6U3|MNMG_ECOLI	-4.77187114	0.003253389
argA	sp|P0A6C5|ARGA_ECOLI	-4.649638457	2.18E-06
yhjE	sp|P37643|YHJE_ECOLI	-4.500028599	0.005992816
yegQ	sp|P76403|YEGQ_ECOLI	-4.482584177	0.015352456
cysN	sp|P23845|CYSN_ECOLI	-3.927062955	7.22E-14
pncB	sp|P18133|PNCB_ECOLI	-3.639270989	6.73E-05
fbp	sp|P0A993|F16PA_ECOLI	-3.600157407	0.023396164
moaA	sp|P30745|MOAA_ECOLI	-3.529794204	0.018342621
rpmC	sp|P0A7M6|RL29_ECOLI	-3.142935813	1.68E-07
ilvN	sp|P0ADF8|ILVN_ECOLI	-3.08821322	0.03765939
aroP	sp|P15993|AROP_ECOLI	-2.833642328	0.021648588
deaD	sp|P0A9P6|DEAD_ECOLI	-2.695068638	0.006647318
ilvB	sp|P08142|ILVB_ECOLI	-2.690257592	1.41E-07
asnA	sp|P00963|ASNA_ECOLI	-2.66746299	0.015909254
ptsG	sp|P69786|PTGCB_ECOLI	-2.510708646	0.000188954
rpmD	sp|P0AG51|RL30_ECOLI	-2.495454148	8.47E-09
ykgM	sp|P0A7N1|RL31B_ECOLI	-2.483011177	0.00644327
gatB	sp|P37188|PTKB_ECOLI	-2.418194429	0.035274735
cs	sp|P0A972|CSPE_ECOLI	-2.352007644	4.54E-08
metA	sp|P07623|META_ECOLI	-2.317452293	0.000139049
der	sp|P0A6P5|DER_ECOLI	-2.267771633	0.0102137
potA	sp|P69874|POTA_ECOLI	-2.183307337	0.03275735
leuA	sp|P09151|LEU1_ECOLI	-1.998105409	1.07E-08
glf	sp|P37747|GLF_ECOLI	-1.97691323	0.029751
tr	sp|P00895|TRPE_ECOLI	-1.943830992	0.005678046
miaB	sp|P0AEI1|MIAB_ECOLI	-1.92205685	0.004244044
pntB	sp|P0AB67|PNTB_ECOLI	-1.852085802	9.85E-06
purF	sp|P0AG16|PUR1_ECOLI	-1.826541229	4.76E-05

lepA	sp|P60785|LEPA_ECOLI	-1.791966706	0.01657399
gatY	sp|P0C8J6|GATY_ECOLI	-1.776699008	0.000182727
purT	sp|P33221|PURT_ECOLI	-1.764435997	0.000643699
prfC	sp|P0A7I4|RF3_ECOLI	-1.76312872	0.012506321
ybiC	sp|P30178|YBIC_ECOLI	-1.727397747	0.01941163
rpsH	sp|P0A7W7|RS8_ECOLI	-1.723379737	2.80E-10
purM	sp|P08178|PUR5_ECOLI	-1.678278829	0.003764
cyoA	sp|P0ABJ1|CYOA_ECOLI	-1.663437618	0.006838543
metL	sp|P00562|AK2H_ECOLI	-1.661017127	0.00181135
leuC	sp|P0A6A6|LEUC_ECOLI	-1.653771358	6.45E-06
pntA	sp|P07001|PNTA_ECOLI	-1.595004247	7.61E-08
trxB	sp|P0A9P4|TRXB_ECOLI	-1.571960722	0.002958769
metH	sp|P13009|METH_ECOLI	-1.565084962	0.000869601
metC	sp|P06721|METC_ECOLI	-1.510217214	0.025144896
rpmF	sp|P0A7N4|RL32_ECOLI	-1.498744569	0.000469522
gyrA	sp|P0AES4|GYRA_ECOLI	-1.448436432	7.72E-05
rpsR	sp|P0A7T7|RS18_ECOLI	-1.418043759	3.03E-05
rpmG	sp|P0A7N9|RL33_ECOLI	-1.381024188	0.006747605
purH	sp|P15639|PUR9_ECOLI	-1.376402854	0.000114658
argI	sp|P04391|OTC1_ECOLI	-1.37321011	0.000772873
rnb	sp|P30850|RNB_ECOLI	-1.364231063	0.003951903
rplT	sp|P0A7L3|RL20_ECOLI	-1.361561823	7.98781E-05
cysS	sp|P21888|SYC_ECOLI	-1.352510933	0.018153582
metK	sp|P0A817|METK_ECOLI	-1.28929395	0.000291382
sdhA	sp|P0AC41|SDHA_ECOLI	-1.284366661	8.12E-05
ydjN	sp|P77529|YDJN_ECOLI	-1.282130778	0.012801159
pyrD	sp|P0A7E1|PYRD_ECOLI	-1.24642368	0.017272295
rpsM	sp|P0A7S9|RS13_ECOLI	-1.231500265	4.82E-05
rpsC	sp|P0A7V3|RS3_ECOLI	-1.228519333	5.14E-06
rplU	sp|P0AG48|RL21_ECOLI	-1.200353979	0.000935979
pliG	sp|P76002|PLIG_ECOLI	-1.192616084	0.023769411
rplB	sp|P60422|RL2_ECOLI	-1.160209361	1.29E-05
rpsA	sp|P0AG67|RS1_ECOLI	-1.154439475	2.19E-06
rplS	sp|P0A7K6|RL19_ECOLI	-1.140490911	0.042048579
rpsT	sp|P0A7U7|RS20_ECOLI	-1.136468494	0.000373058
thrA	sp|P00561|AK1H_ECOLI	-1.131400346	7.55E-06
thrS	sp|P0A8M3|SYT_ECOLI	-1.130800143	0.017957548
rplR	sp|P0C018|RL18_ECOLI	-1.127973054	0.000234204
rplX	sp|P60624|RL24_ECOLI	-1.108686244	0.000297915
aceB	sp|P08997|MASY_ECOLI	-1.103226647	7.72E-05
aroA	sp|P0A6D3|AROA_ECOLI	-1.074448834	0.048313271
rplI	sp|P0A7R1|RL9_ECOLI	-1.074352178	3.31E-05
rplK	sp|P0A7J7|RL11_ECOLI	-1.030031069	0.000940436

argH	sp|P11447|ARLY_ECOLI	-1.029621386	0.010350803
cspC	sp|P0A9Y6|CSPC_ECOLI	-1.010776163	0.00524746
gpmA	sp|P62707|GPMA_ECOLI	1.007836346	0.000278112
gmhA	sp|P63224|GMHA_ECOLI	1.02030343	0.027607596
luxS	sp|P45578|LUXS_ECOLI	1.049588806	0.000506408
rpiA	sp|P0A7Z0|RPIA_ECOLI	1.052561101	0.01318169
pgi	sp|P0A6T1|G6PI_ECOLI	1.065800857	0.000188954
pykF	sp|P0AD61|KPYK1_ECOLI	1.081019653	2.73E-05
mlaC	sp|P0ADV7|MLAC_ECOLI	1.117643099	0.006345313
yfiF	sp|P0AGJ5|YFIF_ECOLI	1.128896995	0.03275735
uspG	sp|P39177|USPG_ECOLI	1.143746641	0.03765939
pgl	sp|P52697|6PGL_ECOLI	1.167828441	0.01318169
deoC	sp|P0A6L0|DEOC_ECOLI	1.174516518	0.018153582
grxB	sp|P0AC59|GLRX2_ECOLI	1.178432467	0.000732045
fbaB	sp|P0A991|ALF1_ECOLI	1.197658464	7.99E-05
adhE	sp|P0A9Q7|ADHE_ECOLI	1.201151692	3.88E-07
degP	sp|P0C0V0|DEGP_ECOLI	1.206061871	0.000278112
tas	sp|P0A9T4|TAS_ECOLI	1.219282681	0.036014767
katG	sp|P13029|KATG_ECOLI	1.220074858	7.01E-05
ribC	sp|P0AFU8|RISA_ECOLI	1.272415628	0.030285161
pmbA	sp|P0AFK0|PMBA_ECOLI	1.273270833	0.007784421
ftnA	sp|P0A998|FTNA_ECOLI	1.301974436	0.010044367
moaB	sp|P0AEZ9|MOAB_ECOLI	1.314241161	0.001746554
wrbA	sp|P0A8G6|NQOR_ECOLI	1.34050881	4.33E-06
hdhA	sp|P0AET8|HDHA_ECOLI	1.365397414	0.014224302
yahK	sp|P75691|YAHK_ECOLI	1.380128931	0.000137547
acnA	sp|P25516|ACNA_ECOLI	1.381383706	7.69E-05
sbp	sp|P0AG78|SUBI_ECOLI	1.410886097	0.001647533
degQ	sp|P39099|DEGQ_ECOLI	1.437968753	0.005431624
tktB	sp|P33570|TKT2_ECOLI	1.45986506	7.28E-07
yjgA	sp|P0A8X0|YJGA_ECOLI	1.470361111	0.0375636
glgP	sp|P0AC86|PHSG_ECOLI	1.489480956	0.004703968
yggE	sp|P0ADS6|YGGE_ECOLI	1.497996423	9.00E-05
mtlD	sp|P09424|MTLD_ECOLI	1.508297143	0.007422869
cbpA	sp|P36659|CBPA_ECOLI	1.520821408	0.040987772
deoB	sp|P0A6K6|DEOB_ECOLI	1.533048098	8.38E-05
ybjP	sp|P75818|YBJP_ECOLI	1.536131134	0.007427731
ybaY	sp|P77717|YBAY_ECOLI	1.541925932	0.00084693
tdcE	sp|P42632|TDCE_ECOLI	1.549713435	0.000108916
thiF	sp|P30138|THIF_ECOLI	1.58507647	0.00235383
hdeB	sp|P0AET2|HDEB_ECOLI	1.585194293	0.001902541
tpiA	sp|P0A858|TPIS_ECOLI	1.585411082	9.28E-09
uspE	sp|P0AAC0|USPE_ECOLI	1.605682754	0.000278112

rraA	sp|P0A8R0|RRAA_ECOLI	1.607904489	0.000417551
yeaY	sp|P0AA91|YEAY_ECOLI	1.609759679	0.001461256
nagD	sp|P0AF24|NAGD_ECOLI	1.651426571	0.020565443
slp	sp|P37194|SLP_ECOLI	1.661057589	0.000127411
osmC	sp|P0C0L2|OSMC_ECOLI	1.671087683	3.90E-06
ycfP	sp|P0A8E1|YCFP_ECOLI	1.676895218	0.000511934
acuI	sp|P26646|ACUI_ECOLI	1.680553338	0.001851227
pflB	sp|P09373|PFLB_ECOLI	1.700478434	9.87E-14
lpoB	sp|P0AB38|LPOB_ECOLI	1.721279546	0.000376072
clpB	sp|P63284|CLPB_ECOLI	1.727347175	1.23E-12
gstB	sp|P0ACA7|GSTB_ECOLI	1.748580068	0.001647533
slt	sp|P0AGC3|SLT_ECOLI	1.751322485	0.015251337
yggN	sp|P0ADS9|YGGN_ECOLI	1.768724665	0.049702565
loiP	sp|P25894|LOIP_ECOLI	1.795763405	0.012616436
pspA	sp|P0AFM6|PSPA_ECOLI	1.803047994	0.000834302
chrR	sp|P0AGE6|CHRR_ECOLI	1.829520642	0.00084693
gstA	sp|P0A9D2|GSTA_ECOLI	1.843282701	2.82E-06
msrA	sp|P0A744|MSRA_ECOLI	1.871059945	0.023254637
dps	sp|P0ABT2|DPS_ECOLI	1.8711205	1.92E-14
yghU	sp|Q46845|YGHU_ECOLI	1.947282377	0.000291495
lldD	sp|P33232|LLDD_ECOLI	1.949858867	0.035748827
yfcH	sp|P77775|YFCH_ECOLI	1.988861376	0.015909254
cdd	sp|P0ABF6|CDD_ECOLI	1.993269202	0.042932089
yeaG	sp|P0ACY3|YEAG_ECOLI	2.011516734	4.21E-11
pqiB	sp|P43671|PQIB_ECOLI	2.013507475	0.028681191
ygaU	sp|P0ADE6|YGAU_ECOLI	2.059465726	3.23E-14
blc	sp|P0A901|BLC_ECOLI	2.064974471	0.011100578
qorA	sp|P28304|QOR1_ECOLI	2.155671369	4.33E-07
curA	sp|P76113|CURA_ECOLI	2.175460559	0.010474873
bfr	sp|P0ABD3|BFR_ECOLI	2.180562547	1.56E-13
yegP	sp|P76402|YEGP_ECOLI	2.284730203	7.89E-10
ugd	sp|P76373|UDG_ECOLI	2.340441236	0.018153582
yceF	sp|P0A729|YCEF_ECOLI	2.382621181	0.040987772
yecA	sp|P0AD05|YECA_ECOLI	2.405409463	0.03275735
bepA	sp|P66948|BEPA_ECOLI	2.421711425	0.000774393
otsA	sp|P31677|OTSA_ECOLI	2.448868257	6.65E-08
katE	sp|P21179|CATE_ECOLI	2.50821371	2.35E-14
hchA	sp|P31658|HCHA_ECOLI	2.50879706	2.75E-12
dkgA	sp|Q46857|DKGA_ECOLI	2.649063918	1.64E-08
ybeL	sp|P0AAT9|YBEL_ECOLI	2.658797186	3.16E-08
ymdB	sp|P0A8D6|YMDB_ECOLI	2.671235984	0.024568779
fruB	sp|P69811|PTFAH_ECOLI	2.672541661	1.42E-05
ydbC	sp|P25906|YDBC_ECOLI	2.711914425	0.046758232

ynhG	sp|P76193|YNHG_ECOLI	2.733690087	3.31E-05
yciE	sp|P21363|YCIE_ECOLI	2.735728026	4.14E-05
ymbA	sp|P0AB10|YMBA_ECOLI	2.798163878	0.036198317
ydcL	sp|P64451|YDCL_ECOLI	2.82774542	2.04E-15
ldhA	sp|P52643|LDHD_ECOLI	2.837647013	2.28E-05
amn	sp|P0AE12|AMN_ECOLI	2.855927832	1.06E-13
yehZ	sp|P33362|YEHZ_ECOLI	2.946432256	0.017149234
mdtE	sp|P37636|MDTE_ECOLI	3.005567607	2.30E-05
gadB	sp|P69910|DCEB_ECOLI	3.026824738	1.75E-33
yhjG	sp|P37645|YHJG_ECOLI	3.114565954	0.004244044
gadC	sp|P63235|GADC_ECOLI	3.122545884	0.000234696
gadA	sp|P69908|DCEA_ECOLI	3.154673417	6.58E-36
ydhF	sp|P76187|YDHF_ECOLI	3.156625723	5.19E-05
yjgR	sp|P39342|YJGR_ECOLI	3.159652222	1.41E-12
yghA	sp|P0AG84|YGHA_ECOLI	3.175685027	1.40E-09
ycaC	sp|P21367|YCAC_ECOLI	3.185383669	2.44E-13
phoE	sp|P02932|PHOE_ECOLI	3.204721908	2.80E-10
ycgM	sp|P76004|YCGM_ECOLI	3.314835257	0.007920581
tam	sp|P76145|TAM_ECOLI	3.330887068	0.010474873
yhbO	sp|P45470|YHBO_ECOLI	3.335162899	0.000187361
phoR	sp|P08400|PHOR_ECOLI	3.473374236	0.001325039
mdaB	sp|P0AEY5|MDAB_ECOLI	3.504985139	1.26E-20
dkgB	sp|P30863|DKGB_ECOLI	3.638374711	5.12E-09
yniA	sp|P77739|YNIA_ECOLI	3.681925301	2.85E-07
gldA	sp|P0A9S5|GLDA_ECOLI	3.74947351	3.13E-05
phnD	sp|P16682|PHND_ECOLI	3.815420505	9.61E-10
ugpQ	sp|P10908|UGPQ_ECOLI	4.003964005	1.04E-06
ahr	sp|P27250|AHR_ECOLI	4.055942555	2.68E-05
pstS	sp|P0AG82|PSTS_ECOLI	4.113208109	3.15E-56
cysQ	sp|P22255|CYSQ_ECOLI	4.144617537	1.22E-07
glsA1	sp|P77454|GLSA1_ECOLI	4.234450197	0.024320745
yciF	sp|P21362|YCIF_ECOLI	4.316219533	0.000228764
ais	sp|P45565|AIS_ECOLI	4.363027397	0.02438333
kefG	sp|P0A756|KEFG_ECOLI	4.489497738	0.01318169
ydcS	sp|P76108|YDCS_ECOLI	4.581943058	0.009304996
phnB	sp|P16681|PHNB_ECOLI	4.606620186	4.21E-11
sodC	sp|P0AGD1|SODC_ECOLI	4.625310091	1.37E-05
arnA	sp|P77398|ARNA_ECOLI	4.698344251	1.36E-11
fic	sp|P20605|FIC_ECOLI	4.74532692	0.001647533
ugpB	sp|P0AG80|UGPB_ECOLI	4.789402823	1.62E-50
phoU	sp|P0A9K7|PHOU_ECOLI	4.829226009	7.34E-29
kdpC	sp|P03961|KDPC_ECOLI	4.927327983	0.001190624
pstB	sp|P0AAH0|PSTB_ECOLI	5.294764534	6.41E-25

yebE	sp|P33218|YEBE_ECOLI	5.774676565	1.18E-14
phoA	sp|P00634|PPB_ECOLI	5.790096911	7.32E-85
phoB	sp|P0AFJ5|PHOB_ECOLI	Inf	8.96E-35
arnB	sp|P77690|ARNB_ECOLI	Inf	8.99E-08
appA	sp|P07102|PPA_ECOLI	Inf	7.69E-05
yedP	sp|P76329|MPGP_ECOLI	Inf	7.72E-05
ugpC	sp|P10907|UGPC_ECOLI	Inf	0.000683993
arnC	sp|P77757|ARNC_ECOLI	Inf	0.008862011
yfcG	sp|P77526|YFCG_ECOLI	Inf	0.018153582
yraR	sp|P45469|YRAR_ECOLI	Inf	0.012911411
yhhA	sp|P0ADX7|YHHA_ECOLI	Inf	0.018724338
phnH	sp|P16686|PHNH_ECOLI	Inf	0.025826417
gspJ	sp|P45761|GSPJ_ECOLI	Inf	0.036463755
PmrA	sp|P30843|PMRA_ECOLI	Inf	0.037433165
alpA	sp|P33997|ALPA_ECOLI	Inf	0.037433165

1189

1190 **Table S2.** Bacteria strains used in this study.

Name	Description	Source
MG1655	*F- λ- ilvG- rfb-50 rph-1*	Lab collection
DH5α	*E. coli* F$^-$ *endA1 glnV44 thi-1 recA1 relA1 gyrA96 deoR nupG purB20 φ80dlacZ*Δ*M15* Δ*(lacZYA-argF)U169*, *hsdR17*($r_K^- m_K^+$), λ^-	Lab collection
Bl21 (DE3)	*E. coli* B F$^-$ *ompT gal dcm lon hsdS*$_B$($r_B^- m_B^-$) [*malB*$^+$]$_{K-12}$(λ^S)	Lab collection
E. coli O157	EHEC, O157:H7	Clinical isolate from Queen Mary Hospital (HK)
UTI-1	UPEC isolated from UTI patients	Clinical isolate from Queen Mary Hospital (HK)
UTI-3	UPEC isolated from UTI patients	Clinical isolate from Queen Mary Hospital (HK)
UTI-4	UPEC isolated from UTI patients	Clinical isolate from Queen Mary Hospital (HK)
UTI-5	UPEC isolated from UTI patients	Clinical isolate from Queen Mary Hospital (HK)
Salmonella ATCC14028	*Salmonella* ATCC14028 wild type	Lab collection
P. aeruginosa PAO1	*P. aeruginosa* PAO1 wild type	Lab collection
AY7010	MG1655 ArnB-3xFLAG	This study
AY0416	MG1655 Δ*lacZ::Km*^{R}	This study

AY4875	MG1655 Δ*arnT*:: *Km*^{R}	This study
AY4860	MG1655 Δ*arnB*:: *Km*^{R}	This study
AY4862	MG1655 Δ*ugd*:: *Km*^{R}	This study
AY4858	MG1655 Δp*mrB*:: *Km*^{R}	This study
AY4859	MG1655 Δ*pmrA*:: *Km*^{R}	This study
AY2741	MG1655 Δ*phoB*:: *Km*^{R}	This study
AY2742	MG1655 Δ*phoR*:: *Km*^{R}	This study
AY7011	MG1655 Δ*pmrB*:: *Km*^{R}*ΔlacZ*	This study
AY7012	MG1655 Δ*pmrA*:: *Km*^{R}*ΔlacZ*	This study
AY7013	MG1655Δ*phoB*:: *Km*^{R}*ΔlacZ*	This study
AY7014	MG1655Δ*phoR*:: *Km*^{R}*ΔlacZ*	This study
AY7015	MG1655 *ΔlacZ, pmrB*^{E36A}	This study
AY7016	MG1655 *ΔlacZ, pmrB*^{E39A}	This study
AY7017	MG1655 Δ*pmrA*	This study
AY7018	MG1655 *pmrB*^{E36A}	This study
AY7019	MG1655 *pmrB*^{E39A}	This study
AY7020	MG1655 Δ*fecA*	This study
AY7021	MG1655 Δ*fepA*	This study
AY7022	MG1655 Δ*entE*	This study
AY7023	MG1655 Δ*fiu*	This study
AY7024	MG1655 Δ*cirA*	This study
AY7025	MG1655 Δ*fecA* Δ*fepA* Δ*entE* Δ*fiu* Δ*cirA*	This study

Table S3. Plasmids used in this study.

Name	Relevant characteristics	Source
pNN387	Single copy plasmid containing NotI and HindIII restriction sites before *lacZ*	Lab collection
pNN387(P*arn-lacZ*)	Ligate promoter of *arn* into NotI/HindIII linearized pNN387	This study
pNN387(P*ugd-lacZ*)	Ligate promoter of *ugd* into NotI/HindIII linearized pNN387	This study
pNN387(P*phoQ-lacZ*)	Ligate promoter of *phoQ* into NotI/HindIII linearized pNN387	This study
pNN387(P*mgtA-lacZ*)	Ligate promoter of *mgtA* into NotI/HindIII linearized pNN387	This study
pET-28a-N	t7 promoter in pET-28a is replaced by araBad promoter	This study
pET-28a-N-3xFLAG	C-terminal 6xHis tag in pET-28a-N is replaced by 3xFLAG tag	This study
pET-28a-N-PmrA-6xHis	Ligate *pmrA* into NcoI/XhoI linearized pET-28a-N	This study
pET-28a-N-PmrA-3xFLAG	Ligate *pmrA* into NcoI/XhoI linearized pET-28a-N-3xFLAG	This study
pET-28a-N-PmrA137TAG-6xHis	Mutate G137 to TAG in pET28A-N-PmrA-6xHis	This study
pEVOL-CouA-RS	Plasmid expression CouA tRNA synthetase	Lab collection
pCAGO	Editing plasmid containing CRISPR-Cas9 and λ-red	Gift from Prof. Changhao Bi